ORNL/TM-2023/3205

Quality Control Methods for Measurement of UCO Kernel Composition and SiC Microstructure

Grant W. Helmreich
Katherine I. Montoya
William F. Cureton
Eddie Lopez-Honorato
Tyler J. Gerczak
John D. Hunn

December 2023

OAK RIDGE National Laboratory

ORNL IS MANAGED BY UT-BATTELLE LLC FOR THE US DEPARTMENT OF ENERGY

ORNL/TM-2023/3205

Nuclear Energy and Fuel Cycle Division

QUALITY CONTROL METHODS FOR MEASUREMENT OF UCO KERNEL COMPOSITION AND SIC MICROSTRUCTURE

Grant W. Helmreich
Katherine I. Montoya
William F. Cureton
Eddie Lopez-Honorato
Tyler J. Gerczak
John D. Hunn

December 2023

Prepared by
OAK RIDGE NATIONAL LABORATORY
Oak Ridge, TN 37831
managed by
UT-BATTELLE LLC
for the
US DEPARTMENT OF ENERGY
under contract DE-AC05-00OR22725

CONTENTS

LIST OF FIGURES

LIST OF TABLES

ABBREVIATIONS

AGR	Advanced Gas Reactor Fuel Development and Qualification Program
ASTM	American Society for Testing and Materials
BSE	backscattered electron
BWXT	BWX Technologies Inc.
GSAS	General Structure Analysis System
MDL	minimum detection limit
NQA	Nuclear Quality Assurance
ORNL	Oak Ridge National Laboratory
QC	quality control
SEM	scanning electron microscope
SiC	silicon carbide
TRISO	tristructural-isotropic
UCO	uranium carbide/uranium oxide
XRD	x-ray diffraction

ACKNOWLEDGEMENTS

The authors would like to acknowledge Daniel Brown, Taylor Duffin, and Nicholas Linneen for advice and assistance in sample preparation as well as helpful discussions in analyzing the gathered data.

ABSTRACT

Quality control (QC) is critically important to tristructural-isotropic (TRISO) particle fuels owing to the complexity of and reliance on the fuel form to contain fission products during irradiation. Characterization methods for particle fuel QC have decades of history and have continued to develop as new insights into fuel performance inform revised fuel specifications and as advances in underlying technologies expand the possibilities of what may be characterized. Two relatively new methods for characterization of TRISO fuels have been published in open literature: optical microscopy image analysis for mixed uranium carbide/uranium oxide (UCO) kernel composition analysis and automated grain boundary detection in backscattered electron (BSE) images of the silicon carbide (SiC) layer in TRISO particles for grain size characterization. Suggestions and guidelines for the application of these methods to TRISO fuel qualification are provided in this report.

1. OPTICAL IMAGE ANALYSIS METHOD FOR UCO KERNEL COMPOSITION

1.1 SPECIFICATION OF UCO KERNEL COMPOSITION

UCO kernels consist of a heterogeneous mixture of uranium carbide ($UC + UC_{2-x}$) and UO_2[1] [1]. Uranium oxide is easy to fabricate, has good stability under irradiation, and retains many fission products as stable oxides. However, oxygen released from a UO_2 kernel by fission of uranium can react with the surrounding carbon-based buffer layer to produce CO. Excess CO results in higher internal pressures [2], corrosion of the SiC layer [3], and migration of uranium-bearing phases into the buffer region [4]. These deleterious effects can be mitigated by the inclusion of some fraction of uranium in the kernel in the form of a carbide to act as in situ getter for oxygen released during fission of uranium present as an oxide. For this purpose, the stoichiometry of the carbide phase does not significantly limit its effectiveness as an oxygen getter because uranium reacts with free oxygen, leaving behind residual carbon. Therefore, calculations may be performed to determine the minimum required fraction of uranium atoms in carbide form to prevent CO production up to a given burnup [5].

Historically, UCO kernel composition has been specified in terms of O/U, C/U, and C+O/U ratios, which are measured for samples of hundreds of kernels [6]. However, these ratios are an indirect measure of the oxide and carbide fractions and specified limits are generally determined based on desired quantity of uranium in carbide form in each kernel and an assumed or measured UC_{2-x} stoichiometry. This approach has three primary issues. First, only the mean kernel composition is measured, not the distribution, potentially allowing some fraction of kernels to have less than the necessary uranium carbide fraction to prevent CO production up to the desired burnup. Second, the relationship between the carbide fraction and the elemental ratios commonly specified are very sensitive to variations in uranium carbide stoichiometry or residual free carbon remaining in the kernel from the conversion process. Third, the measured elemental ratios will shift depending on when the measurements are made because monocarbide, which may exist as the predominant carbide phase in the as-fabricated kernels converts to dicarbide during coating layer deposition and subsequent heat treatment of the fuel compacts.

An improved method for measuring UCO kernel composition has been developed to address these weaknesses and allow the specification to be directly associated with the measured fractions of uranium in oxide and carbide forms. As described in Section 1.2, this method is based on automated image analysis of optical microscopy images taken of polished kernel cross sections. Additional background on the development of the method may be found in the original publication detailing its development [7]. An

[1] UO_2 may be hyperstoichiometric in UCO kernels; however, the variation from balanced stoichiometry is substantially smaller than for UC_{2-x}, and as such it is referred to simply as UO_2 herein.

official data acquisition method has been issued at the US Department of Energy's Oak Ridge National Laboratory (ORNL), allowing the application of this method at a Nuclear Quality Assurance (NQA)-1 level of rigor.

Although the optical analysis method can measure the volume fractions of uranium oxide and uranium carbide on a per-kernel basis, further improvement is still possible. To determine the atomic fraction of uranium present as a carbide, it is also necessary to differentiate the two carbide components so that their different densities and molecular weights can be used in the conversion from measured volume fractions to atomic fractions. This differentiation is currently done by acquiring additional data from x-ray diffraction (XRD) to determine the relative fractions of monocarbide and dicarbide phases. A similar image analysis approach applied to BSE images of kernels with the additional capability to distinguish between the two carbide phases via sensitivity of backscattered electron intensity to density, would allow a more accurate determination of UCO kernel atomic fractions without the need for additional external data.

1.2 STEPS FOR MEASUREMENT OF UCO KERNEL COMPOSITION

1.2.1 Sample Selection

This characterization approach may be performed on either bare kernels or coated particles. Examples of both are given in Section 1.3. Additionally, this procedure may be performed on either an individual batch of material or a composite of multiple batches. When analyzing a composite, extra care should be taken to confirm a singular normal distribution of properties because the gaussian statistics generally applied to variable properties are not accurate for multimodal distributions.

Whether characterizing a single batch or a composite, a subsample of the appropriate size should be taken from the bulk material by a random representative sampling method such as chute splitting or rotary riffling (preferred). The target mass of the sample may be set from a known kernel or particle average mass and the desired number of particles based on the level of statistical sampling. For most fabrication batches, a sample of about 100–300 kernels or particles is sufficient to construct a normal distribution.

1.2.2 Mounting and Polishing

Once an appropriate sample has been identified, kernels or particles should be mounted in a single layer in epoxy to form a materialographic mount. Because of the large number of kernels/particles required for statistical purposes, consideration should be given to how to efficiently image each kernel/particle in the sample. One potential approach is to mount kernels/particles in a square or hexagonal array and use the known positions to automate imaging. Another method is to mount kernels/particles in random positions and use a low-magnification image of the mount to automatically identify kernel positions for subsequent higher magnification imaging of each kernel.

Before grinding and polishing, the mount's height should be measured so that a polish-down distance correction can be applied to the final data. This correction is important to accurately represent the true distribution of phases within the typically heterogenous UCO kernels from images that are not acquired at exactly the kernel midplane. Individual particle polish-down distance can be readily determined if the top and bottom surfaces of the mount are flat. It is not necessary for the surfaces to be parallel, and they typically will not be. Assuming flat surfaces, the mount height is measured at a minimum of three known positions and the polish-down distance as a function of position is determined. It should be noted that the polish-down correction is based on the assumption of roughly spherical kernels and roughly spherical and concentric particles. Uncertainty analysis has shown that minor variations from the ideal case will not substantially affect the analysis results [7].

Grinding and polishing steps should be performed with a focus on maintaining the microstructure of the kernel and keeping a planar surface. Careful polishing is necessary when approaching the midplane of the kernel to ensure that friable material on the outer rim of the kernel is not removed. Particularly in particle samples, vacuum backpotting of the kernel within the buffer layer is necessary. Polish-down distance should be tracked throughout the grinding and polishing steps to obtain a well-polished surface near the approximate midplane of the kernels.

1.2.3 Imaging

Individual images of each kernel should be acquired using an optical light microscope. For particle samples, the full particle must be in the field of view to determine the particle diameter in the imaging plane for the polish-down correction. Optionally, a second set of images at higher magnification may be acquired with only the kernel in the field of view. The coordinates of each kernel on the mount must be recorded along with the images acquired so that the correct polish-down distances may be applied to each. This process is simplified by using an automated sample stage that records the position of each image.

1.2.4 Image Analysis

A detailed description of the image analysis methods used to determine UCO kernel composition from optical microscopy images of kernel cross-sections has been previously published [7]. In summary, the kernel must first be segmented from the surrounding particle or epoxy by using simple thresholding and morphological processing. Then, the oxide phase (bright), carbide phase (gray), and voids (dark) within the kernel may be segmented based on simple thresholding. Areal fractions in the imaging plane can be converted to volumetric fractions in the full kernel by weighting each segmented pixel by the volume of the spherical shell it resides within divided by the area of the annulus in the imaging plane from which it is taken. Removing unnecessary constants, the radially dependent weight *w* may be calculated as follows:

$$w(r) = \frac{r_o^{c3} - r_i^{c3}}{{r_o}^2 - {r_i}^2},$$

where r_o^c and r_i^c are the polish-down corrected outer and inner radii of the pixel, and r_o and r_i are the raw outer and inner radii of the pixel. The polish-down corrected radii r^c may be calculated as follows:

$$r^c = \sqrt{\frac{\left(\overline{R}^2 - p^2\right)^2}{4p^2} + r^2},$$

where $\overline{R}$ is the average radius of the kernel (or the particle if particles were mounted) in the imaging plane, p is the polish-down distance at this location on the mount, and r is the radius being corrected in the imaging plane.

One additional correction that should be applied to the calculated volumetric phase fractions at this point is for the remainder in the center of the kernel that is unobserved because of deviations from the midplane. For typical mounts polished to near midplane, the volume of this region is relatively small—less than 1% of the total kernel volume. However, a straightforward correction may be made by assuming that this region has a composition similar to its immediate surroundings. The radius of this region may be determined using the polish-down correction equation with an imaging plane radius of zero.

Finally, mass fractions of each phase may be calculated from volumetric fractions using the density of each phase. This calculation is straightforward in the case of the oxide phase, but for the carbide phase the density varies slightly with stoichiometry of the dicarbide and significantly between the monocarbide and

dicarbide phases. Consequently, it may be necessary to measure the monocarbide/dicarbide ratio for the carbide phase and the stoichiometry of the dicarbide phase to ensure an accurate density value and thus an accurate mass fraction. These measurements may be performed using XRD or other techniques [7]. Once mass fractions of each phase have been calculated, molar fractions of each element may be calculated based on molecular weights and stoichiometry.

1.3 ADVANCED GAS-COOLED REACTOR SAMPLES USED FOR UCO KERNEL CHARACTERIZATION.

The UCO kernels in archived samples from all four Advanced Gas Reactor Fuel Development and Qualification (AGR) Program irradiation campaigns were characterized in this work.

Archived samples of bare kernels (LEU01-50K) and kernels in coated particles (LEU01-45T—one of the coater batches in the LEU01-46T coated particle composite for the AGR-1 Baseline Fuel) were mounted, polished to near midplane, and imaged using an optical microscope to measure the distribution of UCO kernel composition. The bare kernels and coated particle kernels were from the same BWX Technologies Inc. (BWXT) AGR-1 kernel composite G73D-20-69302, which was measured by BWXT to have a mean C/U ratio of 0.3253, a mean O/U ratio of 1.3613, and a mean density of 10.66 g/cm^3. Underlying measurements on the six kernel batches used to form composite 69302 had mean C/U ratios ranging from 0.278 to 0.385, mean O/U ratios ranging from 1.350 to 1.411, and mean densities ranging from 10.31 to 11.00 g/cm^3 [8, 9]. Further measurement of the kernel composite at ORNL found a mean kernel density of 10.924 g/cm^3 [10]. The higher density measured by ORNL has previously been attributed to the different analysis techniques used by the two laboratories, with the higher ORNL value being a more accurate measurement of the average envelope density of the kernels and the lower BWXT value more closely representing the bulk density of the kernel sample [11].

Archived samples of kernels (LEU04-01K) and kernels in coated particles (LEU09-B01 from BWXT G73J-14-93073A) from the AGR-2 campaign were characterized. The bare kernels and kernels analyzed after coating were both from BWXT AGR-2 kernel composite G73I-14-69307, which was measured by BWXT to have a mean C/U ratio of 0.392, a mean O/U ratio of 1.428, and a mean density of 10.966 g/cm^3 [12]. Underlying measurements on the five kernel batches used to form composite 69307 had mean C/U ratios ranging from 0.39 to 0.40 and mean densities ranging from 10.8 to 11.1 g/cm^3 [13].

Archived samples of kernels (LEU03-01K) and kernels in coated driver-fuel particles (LEU03-10T) from the AGR-3/4 campaign were characterized. The bare kernels and coated kernels were from the BWXT AGR-3/4 kernel composite G73V-20-69303, which was measured by BWXT to have a mean C/U ratio of 0.361, a mean O/U ratio of 1.43, and a mean density of 10.87 g/cm^3 [14]. This composite was formed by mixing two kernel batches, but underlying elemental ratio data for those batches is not available [15]. Density measurements taken at ORNL on the kernel composite found a mean density of 11.098 [16, 17].

The only available AGR-5/6/7 samples for characterization were archived compacts, so particles were deconsolidated from a compact in hot nitric acid to extract material. It is known that the coating process results in conversion of some UC in the as-fabricated kernels into UC_{2-x} due to exposure to elevated temperature in the presence of excess carbon. Compacting at 1800°C may have further shifted the chemistry away from the monocarbide to the dicarbide. The kernels in the coated particles used to make the AGR-5/6/7 compacts were from BWXT AGR-5/6/7 kernel composite J52R-16-69317, which was measured by BWXT to have a mean C/U ratio of 0.370, a mean O/U ratio of 1.441, and a mean density of 11.048 g/cm^3 [18]. Underlying measurements on the six kernel batches used to form composite 69317 had mean C/U ratios ranging from 0.33 to 0.41, mean O/U ratios ranging from 1.36 to 1.48, and mean densities ranging from 10.94 to 11.09 g/cm^3 [19].

1.4 SUPPORTING CHARACTERIZATION RESULTS FOR UCO KERNELS

Although the primary focus of this work was establishing a method for measurement of UCO phase composition based on optical microscopy analysis, additional characterization was performed using XRD, electron microscopy, and Raman spectroscopy. These results provide context for the phases present in UCO kernels and confirm the accuracy of the measurement method.

1.4.1 X-ray Diffraction of UCO Kernels from AGR Kernels and Particles

Kernels in archived coated particle samples from all four AGR irradiation campaigns were analyzed by XRD. Furthermore, archived uncoated kernels from AGR-1, AGR-2, and AGR-3/4 were also analyzed. TRISO-coated kernels were isolated by mechanically removing layers using a uniaxial press. TRISO particles were loaded into the center of a ring with a height somewhat less than the particle diameter, and force was applied until the particles cracked. This process facilitated removal of the layers while keeping the kernels intact. Approximately 50 mg of ground kernels were placed on zero-diffraction background SiO_2 disks, held in place with 8 μm Kapton foil, and measured using a Bruker D2 Phaser and a copper Kα source (1.5406 Å).

As shown in Figure 1, the as-fabricated AGR-1 kernels consisted predominantly of UO_2 and UC with faint peaks corresponding to UC_2. However, during the coating process, a reaction with the surrounding buffer layer at elevated temperature converted most of the original UC to UC_2. This result is consistent with prior reporting on kernel behavior during coating [20]. A similar result was observed for kernels and particles from AGR-2 and AGR-3/4; the main distinction was a larger initial fraction of UC_2, as shown in Figure 2. Bare kernels from AGR-5/6/7 were not available for analysis; however, the coated particle kernel results correspond well with those of the prior irradiation campaigns.

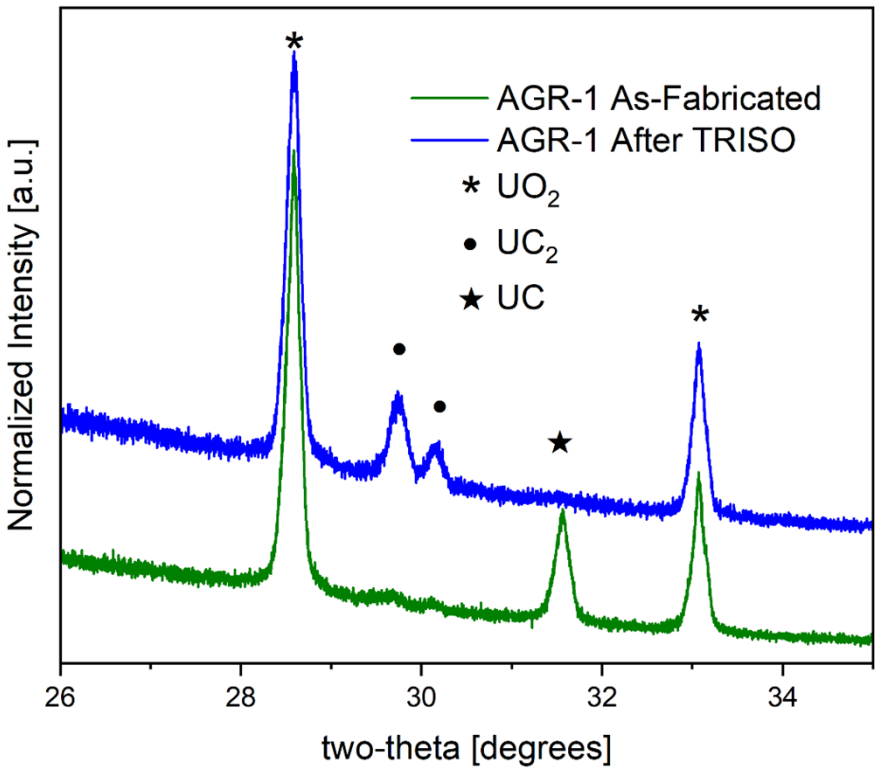

Figure 1. XRD results for AGR-1 kernels as-fabricated (green) and after TRISO coating (blue), showing conversion of UC into UC_2.

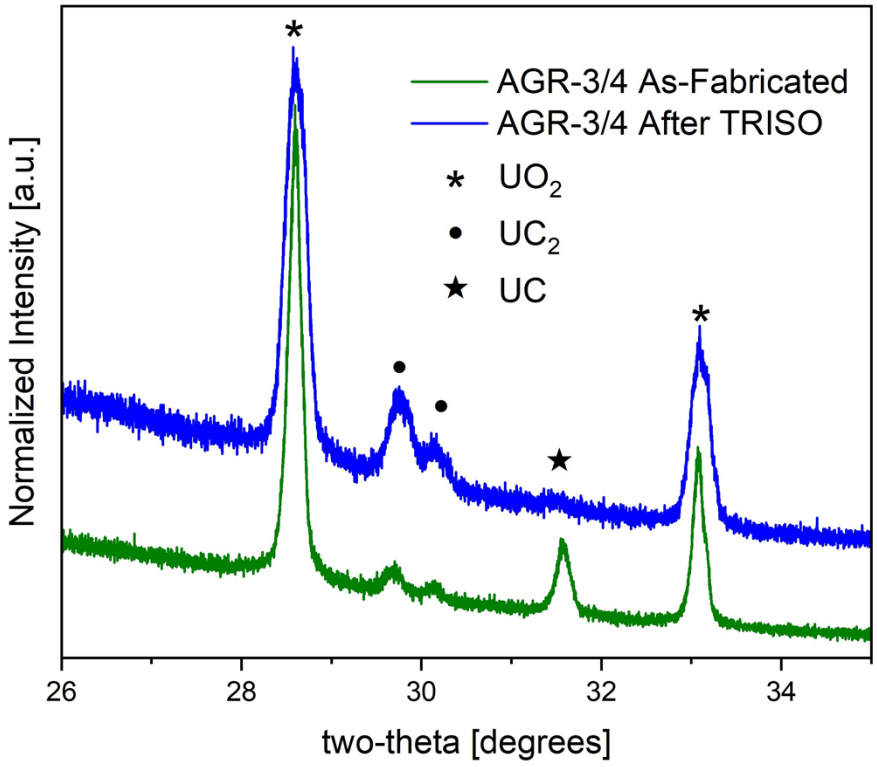

Figure 2. XRD results for AGR-3/4 kernels as-fabricated (green) and after TRISO coating (blue), showing a greater initial fraction of UC_{2-x} compared with AGR-1 (Figure 1) but similar final conversion of UC to UC_{2-x} in particles.

Lattice parameters and phase composition were extracted via Rietveld refinement using the General Structure Analysis System (GSAS)-II software with UO_2 used as the standard [21, 22]. Phase composition results are shown in Table 1. As expected from the data, the as-fabricated kernels contained predominantly UO_2 with either mostly UC and some UC_{2-x} (AGR-1) or a near-even mix of UC and UC_{2-x} (AGR-2 and AGR-3/4). In the particle samples, any residual UC was below the minimum detection limit (MDL) of the analysis, which was approximately 3 wt %. If any residual UC was in a particularly fine grain structure, then it would have been even less detectable by XRD. Lattice parameters and theoretical densities for each phase were calculated and are presented in Table 2.

Table 1.Weight fractions of each phase detected by XRD analysis in AGR kernels before and after coating

		UO_2		UC		UC_2	
		wt %	% err.	wt %	% err.	wt %	% err.
AGR-1	Kernels	70.37	0.15	24.91	0.14	4.72	0.00
	TRISO	69.01	0.24	<MDL	<MDL	30.99	0.24
AGR-2	Kernels	72.05	0.09	13.04	0.09	14.91	0.10
	TRISO	77.29	0.31	<MDL	<MDL	22.71	0.31
AGR-34	Kernels	71.00	0.22	17.18	0.21	11.82	0.25
	TRISO	73.05	0.28	<DL	<DL	26.95	0.28
AGR-567	TRISO	69.61	0.27	<MDL	<MDL	30.39	0.27

Table 2. Lattice parameters (a_0) and theoretical densities for each phase detected by XRD analysis in AGR kernels before and after coating

		UO_2		UC		UC_2	
		a_0 (Å)	Density (g/cm^3)	a_0 (Å)	Density (g/cm^3)	a_0 (Å)	Density (g/cm^3)
AGR-1	Kernels	5.4685	10.97	4.9591	13.62	3.5270	11.66
	TRISO	5.4691	10.96	<MDL	<MDL	3.5205	11.72
AGR-2	Kernels	5.4703	10.96	4.9583	13.62	3.5290	11.66
	TRISO	5.4735	10.94	<MDL	<MDL	3.5249	11.65
AGR-34	Kernels	5.4704	10.96	4.9599	13.61	3.5351	11.63
	TRISO	5.4685	10.97	<MDL	<MDL	3.5198	11.73
AGR-567	TRISO	5.4705	10.96	<MDL	<MDL	3.5235	11.68

1.4.2 BSE Imaging of UCO Kernels from AGR Kernels and Particles

BSE images of as-fabricated UCO kernels and UCO kernels after TRISO coating from the various AGR irradiation campaigns are shown in Figure 3–Figure 7. As expected based on the XRD results presented in Section 1.4.1, the as-fabricated UCO kernels consisted of a heterogenous mixture of UO_2 and uranium carbide: the carbide phase consisted primarily of UC with little (AGR-1) or moderate (AGR-2 and AGR-3/4) UC_{2-x}. In the case of predominantly UC, as shown in Figure 3, small amounts of UC_{2-x} tended to form in small globular pockets within the UC. At higher fractions, as shown in Figure 5–Figure 6, the UC_{2-x} formed into Widmanstätten patterns of platelets. This behavior has been previously observed for uranium carbide in general [23] as well as for UCO kernels [16, 20].

As shown for AGR-1 kernels in Figure 3, the structure of the as-fabricated kernels comprised a large central region of mixed oxide and carbide surrounded by an outer rind of uranium oxide. As shown for AGR-1 kernels in Figure 4, most of the pre-existing UC was converted into UC_{2-x}, leaving only a tertiary UC phase behind in the form of thin striations in the UC_{2-x} grains. Similar observations were evident for AGR-2 kernels (Figure 5) and AGR-3/4 kernels (Figure 6) before and after coating; and this conversion is implied for AGR-5/6/7 kernels (Figure 7), which were only observed after coating. This process of carbide conversion during coating and the resulting structure of the carbide phase has been noted previously [20]. The relatively small fraction of this residual UC and the fineness of its structure account

for the lack of a distinct peak in the XRD results. In addition to the conversion from UC to UC_{2-x}, a carbide skin formed along the outer edge of the kernels during TRISO coating. Based on the density of the monocarbide striations, the composition of the carbide skin appears to be consistent with the carbide in the inner mixed region.

Previous studies have concluded that the mechanism for carbide transformation during coating was conversion in the inner mixed region of UC to UC_{2-x} + UO_2 coupled with reaction of carbon in the buffer layer with the outer kernel to convert UO_2 into UC_2. This process conserves the total amount of uranium in carbide form while increasing the C/U ratio [20] under the general constraints that oxygen is mostly retained in the kernels during coating and the uranium oxide is near stoichiometric UO_2.

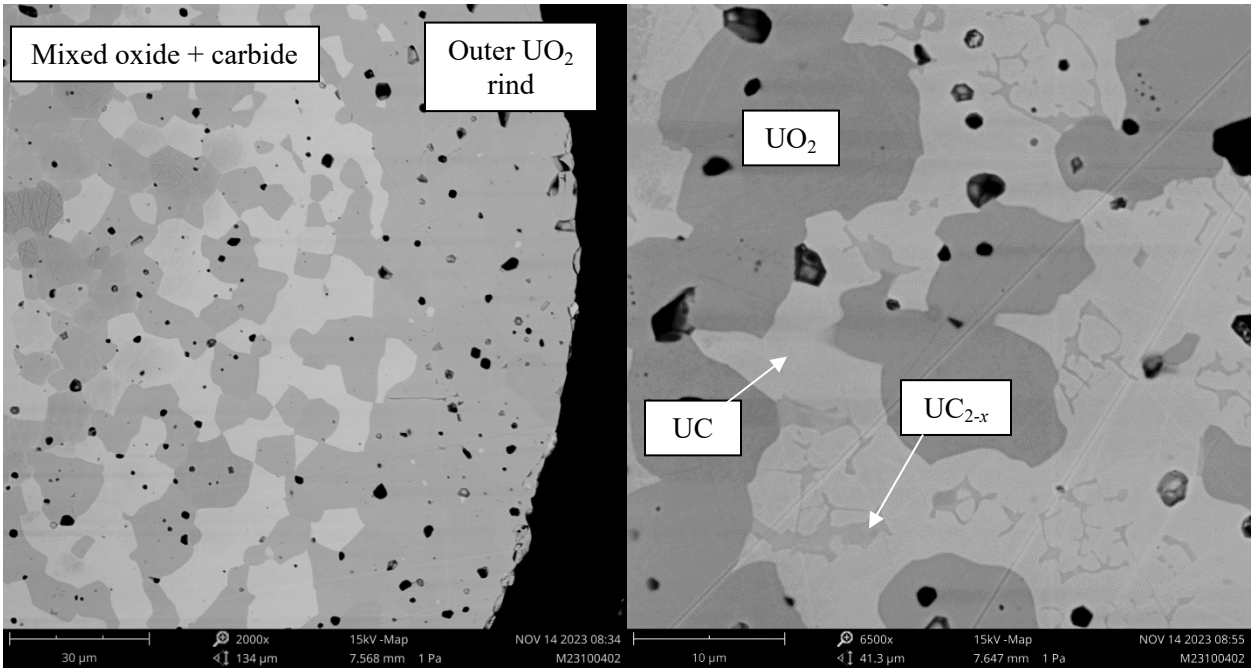

Figure 3. BSE images from an as-fabricated AGR-1 kernel, showing UO_2 and UC with small pockets of UC_{2-x}.

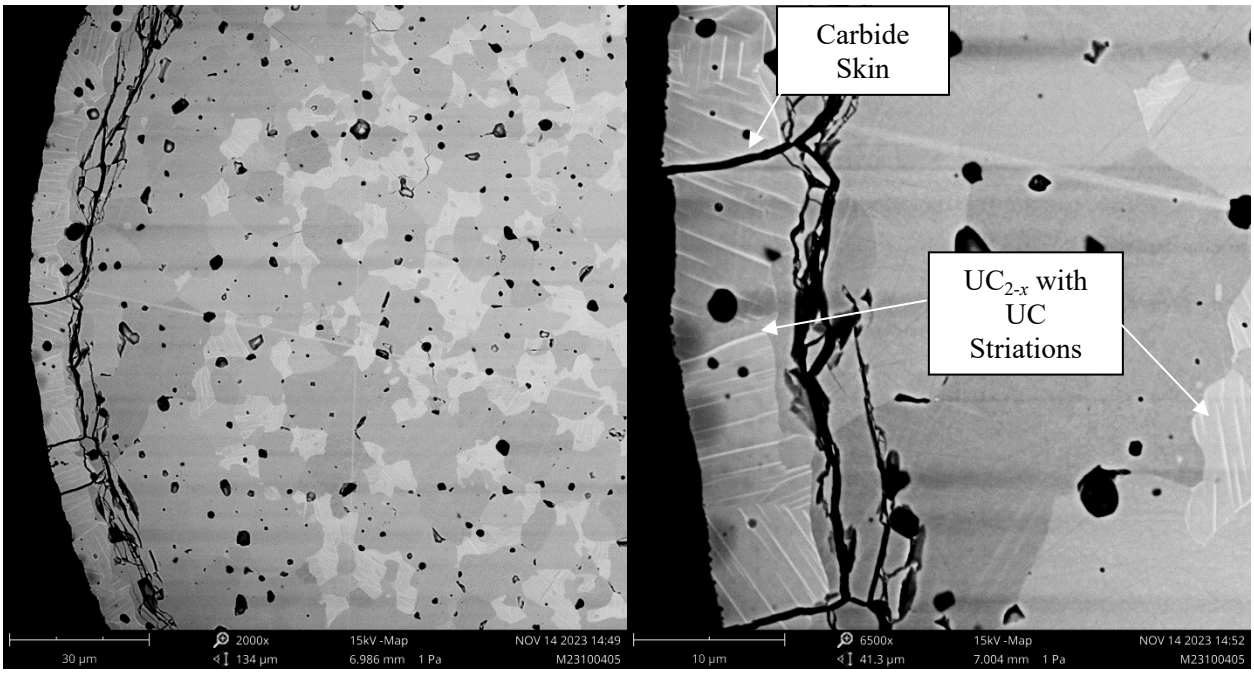

Figure 4. BSE images from an AGR-1 kernel after coating, showing the formation of a carbide skin on the outside of the kernel and conversion of most UC to UC_2.

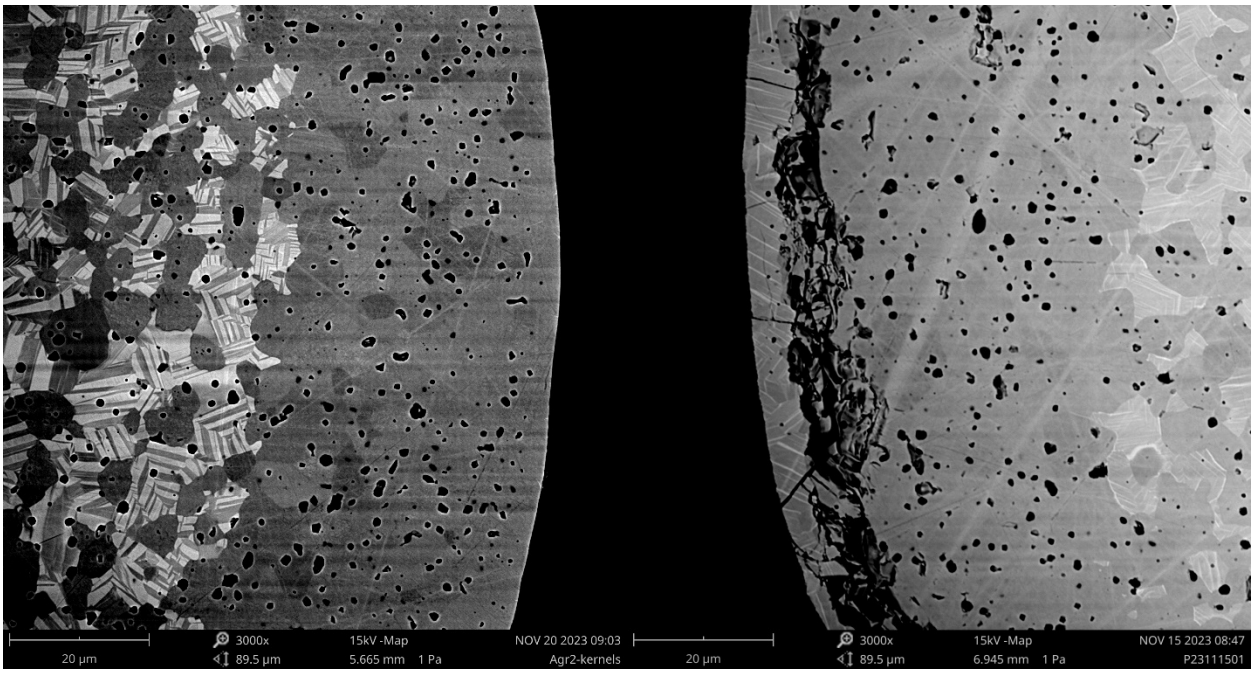

Figure 5. BSE images from (left) an as-fabricated AGR-2 kernel and (right) an AGR-2 kernel after coating.

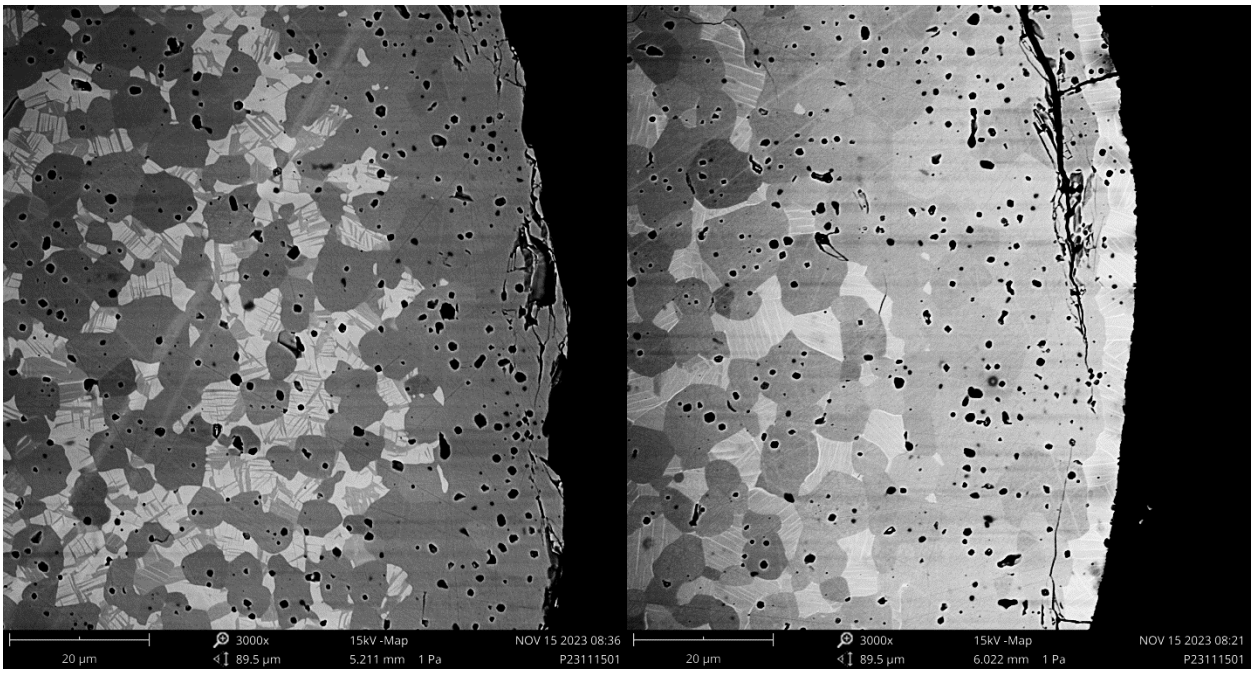

Figure 6. BSE images from (left) an as-fabricated AGR-3/4 kernel and (right) an AGR-3/4 kernel after coating.

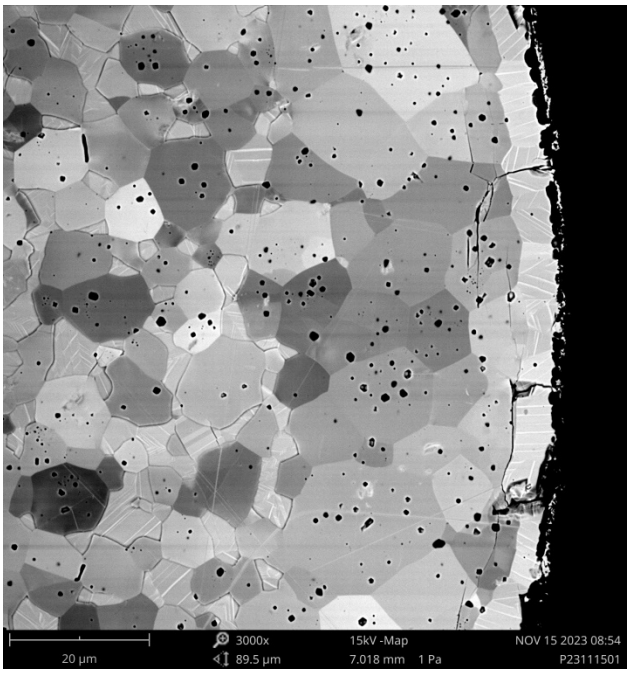

Figure 7. BSE image from an AGR-5/6/7 kernel after coating.

1.5 UCO COMPOSITION RESULTS FOR AGR PARTICLES

The optical microscopy image analysis method described in Section 1.2 was applied to archived material from the AGR-1, AGR-2, AGR-3/4, and AGR-5/6/7 irradiation campaigns. In each of these campaigns, the fuel specification on UCO kernel composition was based on bulk elemental ratios, and no quantitative data on the distribution of phase fractions between kernels were generated. However, the possibility of

kernel-to-kernel compositional variation was acknowledged and addressed via qualitative optical inspection of kernel cross sections, with a requirement in all AGR fuel specifications to demonstrate evidence that both oxide and carbide phases were present in samples drawn from each kernel batch. Because of the extensive postirradiation examination studies that have been completed using these AGR fuel specimens, a more complete understanding of the underlying material is of great interest. In some cases, archived coated particles and as-fabricated kernels were both available, whereas in others, only particle archives were available for analysis.

Examples of the optical micrographs and their automated segmentations for bare kernels and coated kernels are given in Figure 8 and Figure 9, respectively. The segmented images shown were generated for every kernel analyzed and were reviewed by a trained operator to confirm their accuracy.

The phase densities calculated using XRD and presented in Table 2 were used as an input for each analysis, although only minor variations in density were observed between samples and theoretical densities could be used in practice. The relative abundance of UC to UC_{2-x} within the carbide phase of as-fabricated kernels was a more significant input from XRD, using the values in Table 1 for bare kernels. For kernels after coating, the BSE images shown in Section 1.4.2 demonstrate that some residual UC remained after coating albeit in quantities below the detection limits of XRD. Therefore, the carbide in those samples was assumed to be 10 wt % UC and 90 wt % UC_2 (i.e., a sample with 30% carbide was assumed to have 3% UC and 27% UC_{2-x}). Finally, the stoichiometry of the UC_{2-x} phase was set to 1.7 for all samples. Generally, UC_{2-x} tends to be hypostoichiometric, and this value was determined based on the measured C/U and O/U ratios for the bulk kernels coupled with the relative monocarbide abundance from Table 1.

The relative UC abundance and the UC_{2-x} stoichiometry are very important for calculating an atomic ratio of C/U as has historically been specified for UCO kernels; however, these values are far less important to the calculation of the atomic percentage of uranium in carbide form. If the approximate density of the UC_{2-x} phase is known, then its stoichiometry does not matter at all to this calculation, and the relative abundance of UC matters much less because the slight increase in density over UC_{2-x} has much less of an effect than the large difference in C/U between the two phases.

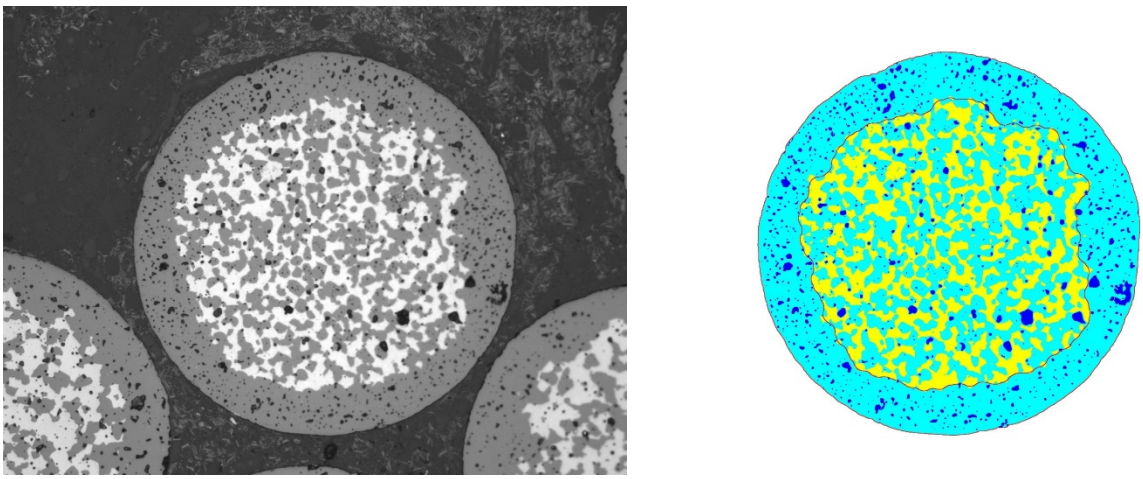

Figure 8. (left) Representative optical micrograph of an as-fabricated kernel from AGR-1 and (right) the corresponding segmented image generated by the image analysis software, showing carbide (yellow), oxide (light blue), and voids (dark blue).

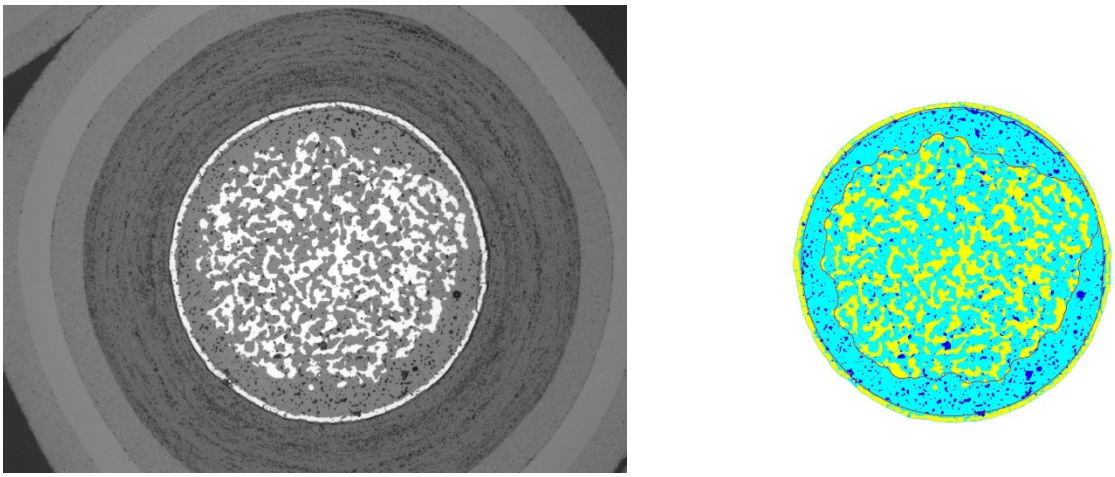

Figure 9. (left) Representative coated kernel from AGR-1 and (right) corresponding segmented image, showing carbide (yellow), oxide (light blue), and voids (dark blue).

As described in the original publication detailing the software development and analysis method [7], optical image analysis of UCO kernels provides a large amount of data on a per-kernel basis, including atomic ratios, phase volume fractions from which mass fractions are derived, and the dimensions of geometric features such as the thickness of the oxide rind and the carbide skin (if present). To demonstrate some of the parameters that may be measured, histograms showing the distribution of key parameters are given in Figure 10–Figure 13. Figure 10–Figure 12 show the distributions of C/U, O/U, and envelope density of the AGR-3/4 bare kernels. These parameters are commonly used in the kernel specification for UCO TRISO fuels. Figure 13 shows the distribution of atomic percentage of uranium that is present in carbide form. This parameter is more closely tied to the specification basis of ensuring an appropriate amount of getter for CO is present in the kernel for the anticipated burnup, and it does not vary significantly with the carbide stoichiometry.

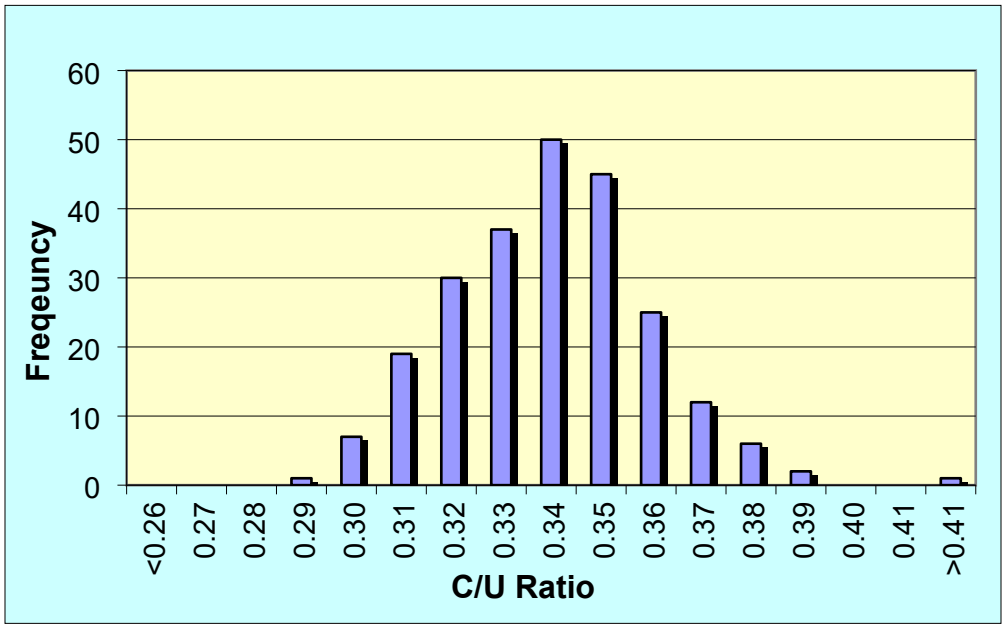

Figure 10. C/U ratio for bare AGR-3/4 kernels as measured as determined by optical image analysis.

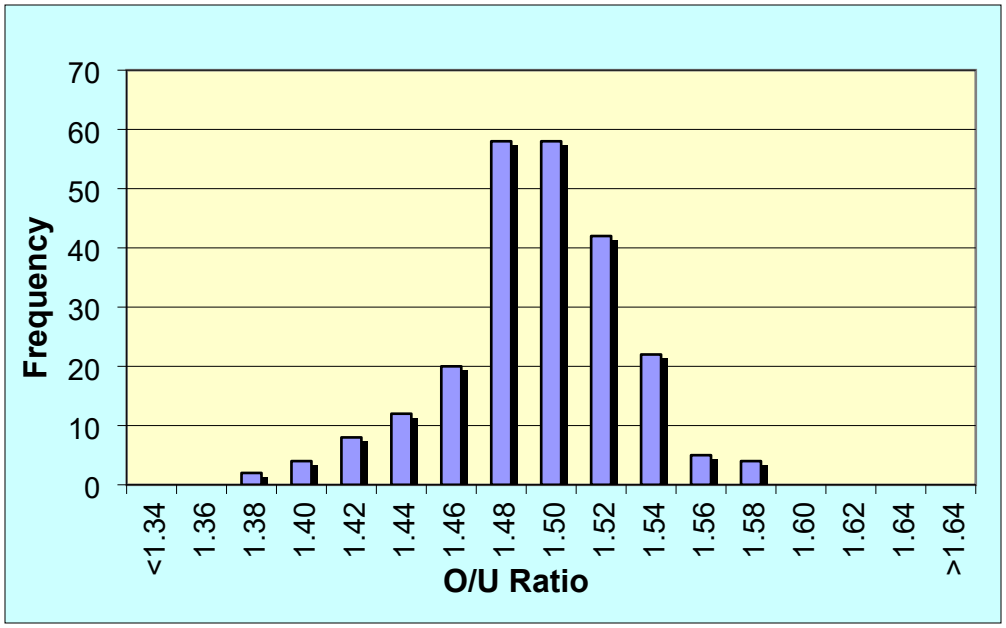

Figure 11. O/U ratio for bare AGR-3/4 kernels as measured as determined by optical image analysis.

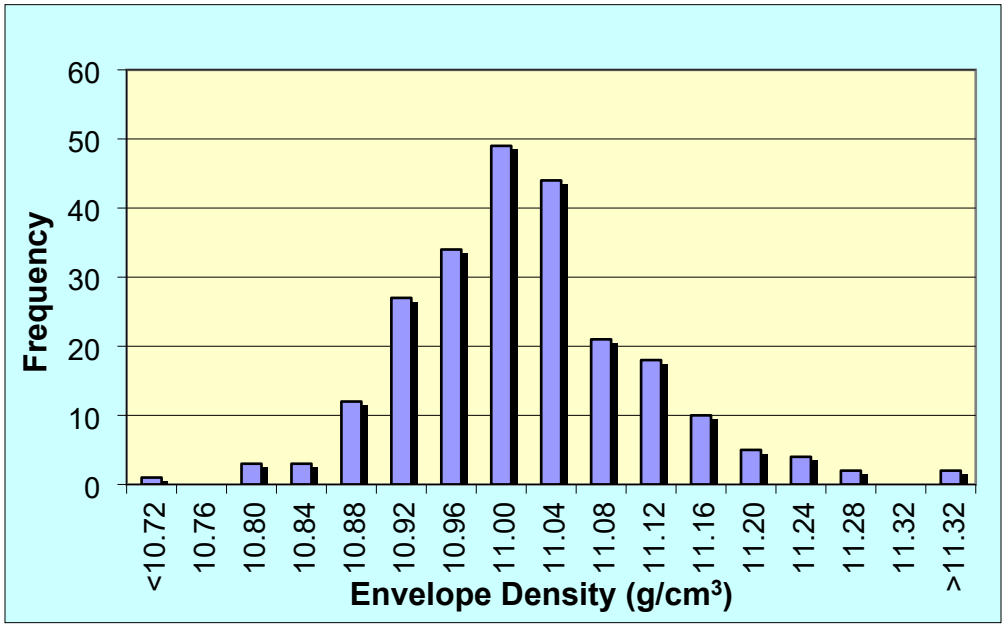

Figure 12. Envelope density calculated from constituent phases for bare kernels from AGR-3/4 as determined by optical image analysis.

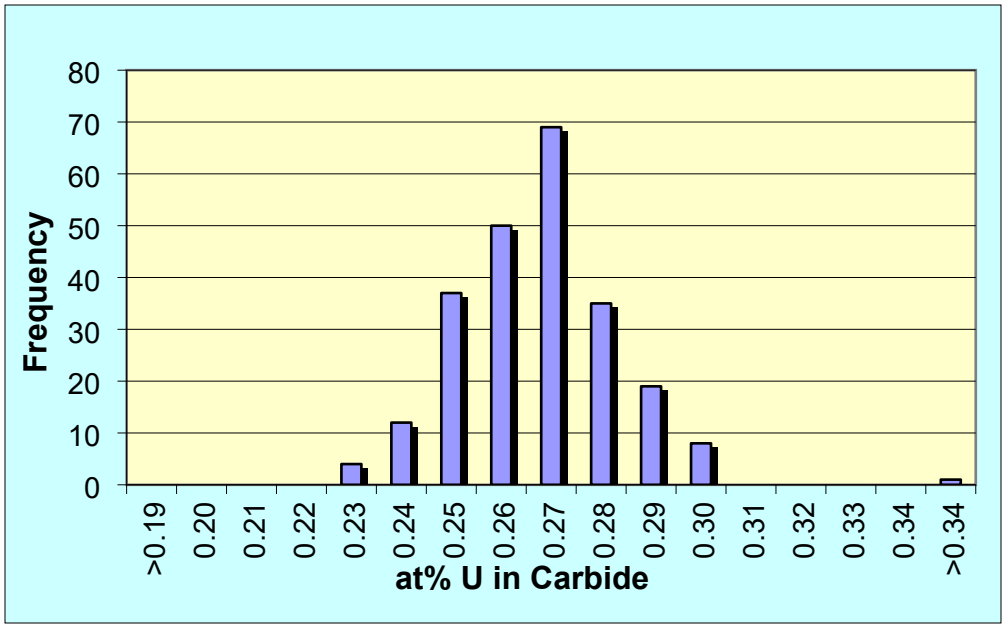

Figure 13. Atomic percentage of uranium present in carbide form for bare kernels from AGR-3/4 as determined by optical image analysis.

The previously published bulk characterization results for the bare UCO kernels, along with the results from this work using XRD and optical image analysis, are provided in Table 3. Some parameters, such as atomic ratios in the case of XRD, were calculated from the measured parameters using the aforementioned assumption that the UC_{2-x} phase had a stoichiometry of 1.7. The apparent atomic percentage of uranium in carbide form was calculated from the BWXT bulk chemistry data by assuming an oxide stoichiometry of 2:1 with the remaining uranium being present in carbide form. The density of the kernels could not be calculated from XRD without data on the void fraction.

Although the data from BWXT and XRD analysis were limited to measurements of bulk values, the image analysis data include statistical measurements of the distribution for each parameter. Thus, the associated standard deviation is provided alongside the mean measured values.

Table 3. Comparison of UCO kernel characterization results from bulk analyses at BWXT and ORNL, bulk powder XRD, and individual kernel optical image analysis

Material source	Data source	C/U	O/U	Density (g/cm^3)	Atom % U in carbide
AGR-1 kernels	Bulk Analysis	0.325 [0.278–0.385]	1.361 [1.350–1.411]	10.9 (ORNL)	0.319
	XRD	0.345	1.377	—	0.312
	Image analysis	0.298 (0.034)	1.462 (0.061)	10.8 (0.2)	0.269 (0.030)
AGR-1 particles	XRD	0.521	1.360	—	0.320
	Image analysis	0.435 (0.036)	1.466 (0.044)	10.3 (0.3)	0.267 (0.022)
AGR-2 kernels	Bulk Analysis	0.390 [0.39–0.40]	1.430	11.0	0.285
	XRD	0.399	1.417	—	0.292
	Image analysis	0.363 (0.027)	1.447 (0.041)	11.0 (0.1)	0.276 (0.021)
AGR-2 particles	XRD	0.383	1.529	—	0.236
	Image analysis	0.413 (0.022)	1.492 (0.027)	10.7 (0.1)	0.254 (0.013)
AGR-3/4 kernels	Bulk Analysis	0.361	1.430	11.1 (ORNL)	0.285
	XRD	0.388	1.393	—	0.303
	Image analysis	0.335 (0.022)	1.476 (0.034)	11.0 (0.1)	0.262 (0.016)
AGR-3/4 particles	XRD	0.454	1.442	—	0.279
	Image analysis	0.401 (0.026)	1.507 (0.032)	10.8 (0.1)	0.246 (0.016)
AGR-5/6/7 kernels	Bulk Analysis	0.370 [0.33–0.41]	1.441 [1.36–1.48]	11.0	0.280
AGR-5/6/7 particles	XRD	0.511	1.372	—	0.314
	Image analysis	0.416 (0.045)	1.489 (0.055)	10.9 (0.1)	0.255 (0.028)

Note: The associated standard deviation for the measured samples is included in round parentheses for the ORNL image analysis data and represents the kernel-to-kernel variation in the measured composite.
Note: The spread in the BWXT measured average atomic ratios for each kernel batch in the composite is included in square brackets, where available, and represents the extent of batch-to-batch variability in the mean values.

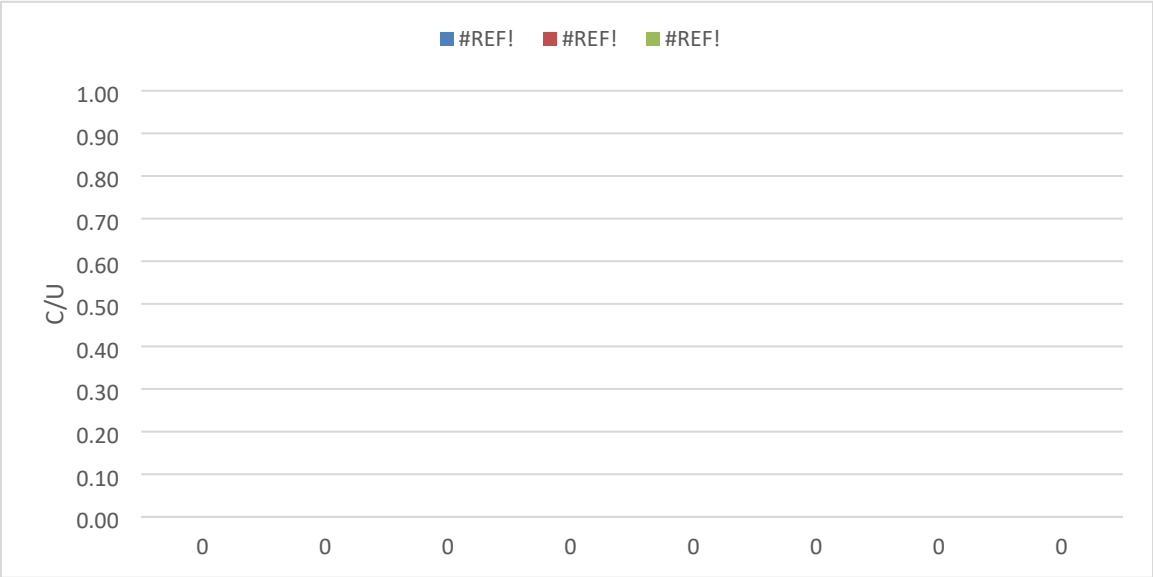

Figure 14. Graphical comparison of measured C/U values from each method for AGR materials.

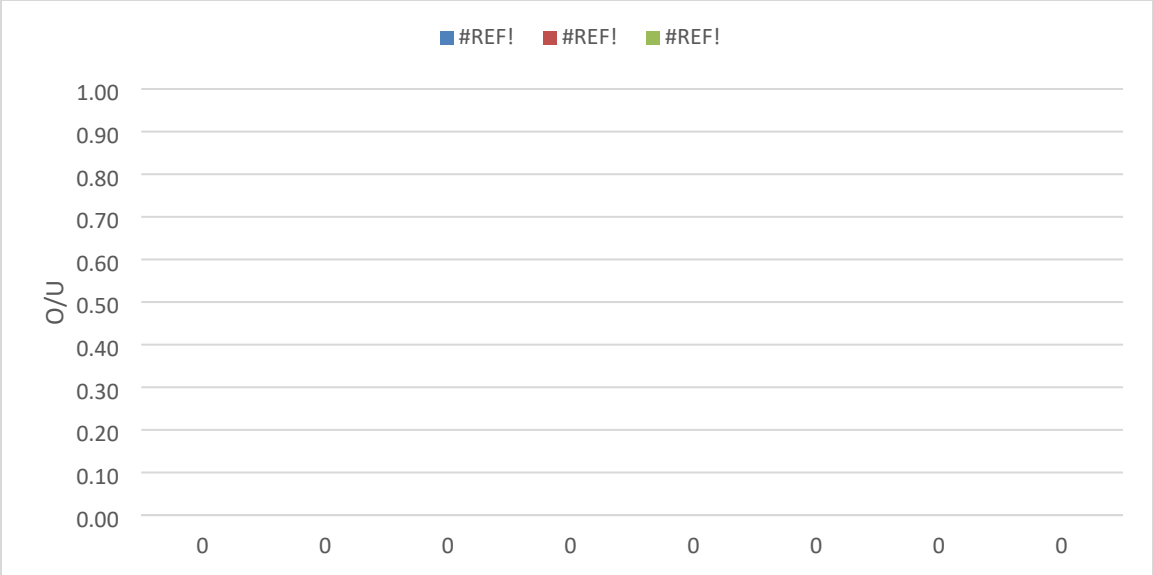

Figure 15. Graphical comparison of measured O/U values from each method for AGR materials.

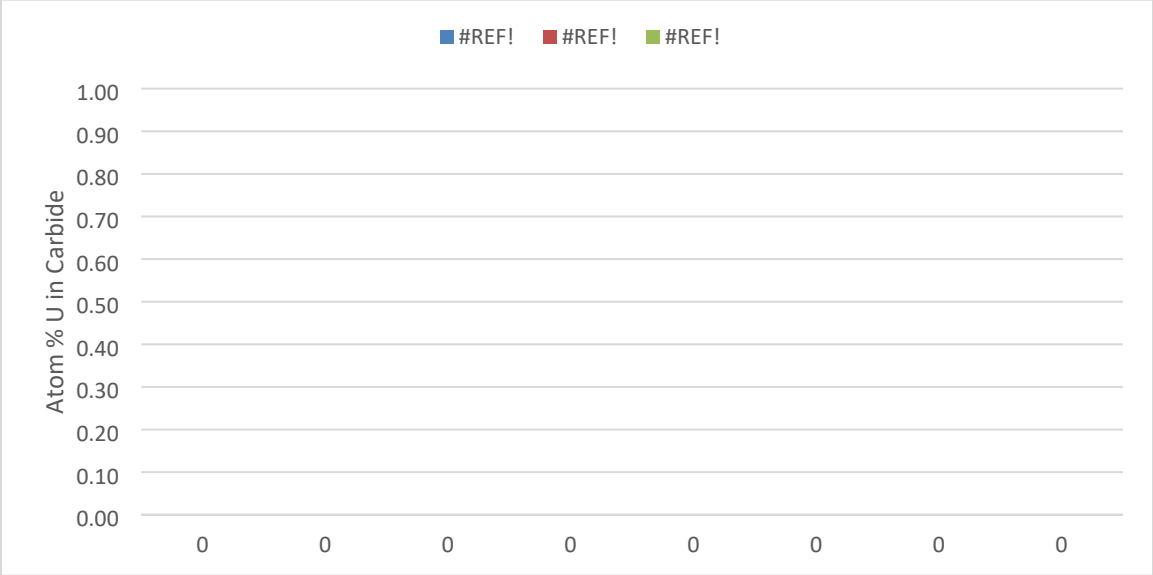

Figure 16. Graphical comparison of measured atomic percentage of uranium in carbide form from each method for AGR materials.

The results reported in Table 3 and shown graphically in Figure 14-Figure 15 show a good general agreement between the various data sources for each material source despite some variation. This variation in results is expected given the assumptions and errors inherent in each measurement method. The bulk chemical measurements made on UCO kernels by BWXT were based on total content of each element, and loose carbon that may remain within the kernels cannot be differentiated from carbon in uranium carbide. The XRD and optical image analysis both rely on an assumed dicarbide stoichiometry for calculation of C/U, and although BSE imaging of kernels in coating particles confirms the presence of UC, the peak is below the detection limit for quantification in XRD. These issues with optical analysis are significantly reduced if the specified parameters are changed from atomic ratios (C/U, O/U and C + O/U) to the atomic percentage of uranium in carbide form. Optical image analysis provides a direct

measurement of volumetric percentage of uranium carbide, and the conversion from volumetric percentage of uranium carbide to atomic percentage of uranium is significantly less sensitive to additional variable inputs (e.g., the fraction of UC within the carbide phase and the stoichiometry dependent density of UC_{2-x}).

Some trends may be observed between the different measurement methods. Measured C/U ratios were generally higher for XRD than for image analysis, with bulk analysis results falling between the two when available (for kernel samples). The opposite trend was observed for O/U ratios, with the highest values observed for image analysis, followed by bulk analysis, then XRD. This inverse relationship is expected given a stable oxide stoichiometry and will be magnified as the relative fraction of UC to UC_{2-x} increases. Given the aforementioned uncertainties and potential systematic errors involved in each of the analysis methods, it is difficult to ascertain which best represents the true stoichiometry of the UCO kernels; however, uncertainty in the measurement methods used may be taken into account when establishing the basis for a kernel stoichiometry specification.

Comparison of the bare and coated kernel data within each measurement method is also interesting. For AGR-1, which had a relatively high fraction of UC in the bare kernels, the at% U in carbide form was observed to be essentially identical before and after coating by both XRD and image analysis. This is consistent with the understood mechanism of kernel conversion during coating in which UC is converted into UC_{2-x} by incorporation of carbon from the buffer layer, but the relative fractions of carbide and oxide are unchanged [20]. However, for AGR-2 and AGR-3/4, both of which had a more even mixture of UC and UC_{2-x} in the bare kernels, the at% U in carbide form decreased from the bare kernels to the coated particles. It is likely that this apparent decrease was due to the loss of some of the friable carbide skin which forms around the outside of the kernel during coating. The greater starting UC fraction in the bare kernels from AGR-1 resulted in the formation of a thicker carbide skin in the coated particles, which may have been more resistant to breaking away during sample preparation for XRD and image analysis. Care was taken to retain as much of the carbide skin as possible, and optical images with significant portions of carbide skin missing were rejected; however, there appears to have been a systematic bias in the measurements of coated kernels due to this issue.

1.6 UCO PHASE ANALYSIS CONCLUSIONS AND RECOMMENDATIONS

A new method to measure the composition of UCO kernels on an individual kernel basis has been established. This method is based on image analysis of optical microscopy images of kernel cross sections and may be applied to either bare or coated kernels. The new method provides statistical data on the distribution of uranium carbide within the population of kernels, enabling potential specification of kernel chemistry as a variable property to ensure that an acceptable fraction of the particle population is within the desired range of each phase present. Finally, the new method supports shifting the specified parameters of UCO kernel composition from atomic ratios, which depend on the stoichiometry of the carbide phase, to the atomic percentage of uranium present in carbide form, which is more closely connected to the basis of including uranium in the form of a carbide as a getter for oxygen released by uranium oxide fission. This shift away from specifying atomic ratios has an additional inherent advantage in that C/U ratios are highly sensitive to both the stoichiometry of uranium dicarbide and the presence of uranium monocarbide and are known to shift after coating due to monocarbide conversion. These sensitivities and variabilities in C/U potentially necessitate additional measurement after coating and compacting or the use of additional analyses to correct for deviations in the as-fabricated kernel carbide stoichiometry from a UC_2 stoichiometry that was apparently assumed in the basis for the originally specified C/U ratio [6].

While the optical image analysis method may be applied to either bare or coated kernels, it is recommended that only image analysis of bare kernels be considered for QC measurement purposes.

While measurements on coated particles are useful for process analysis and may be instructive in refinement of the specification, those measurements have substantially greater inherent uncertainty due to greater sensitivity to faceting and non-concentricity of the kernel on polish-down correction as well as the challenge of friable carbide skin pullout during polishing. Both of these sources of uncertainty may be minimized in a laboratory setting by taking extreme care in sample selection and preparation, but these measures are likely inappropriate for an industrial QC program. This limitation is not an issue if the specification on kernel chemistry is made in terms of the atomic percentage of uranium present in carbide form, as this parameter should not change due to the conversion of UC to UC_{2-x} during coating.

The primary limitation of the new optical image analysis method for UCO kernel phase analysis is the inability to differentiate between UC and UC_2 without additional analyses using more advanced scientific equipment and data processing. At present, this limitation is addressed by using XRD and BSE image analysis to establish the overall ratio of these phases; however, a better solution for future development would be to extend the base image analysis method from optical microscopy images to BSE images in which the two carbide phases may be quantitatively segmented. If performed using a basic benchtop scanning electron microscope (SEM), then this method would still be appropriate for rapid analysis in an industrial setting, and it would remove the uncertainty inherent in assuming an even ratio of UC_{2-x} and UC in all kernels within a batch.

2. BSE IMAGE ANALYSIS METHOD FOR SIC MICROSTRUCTURE

2.1 SPECIFICATION OF SIC MICROSTRUCTURE

Each coating layer of TRISO particles is important to overall fuel performance. The SiC layer is the primary barrier to release of fission products not contained within the kernel. Strength and resistance to fission product diffusion both depend in some measure on the microstructure of the SiC layer. Consequently, fuel specifications have commonly included process or property requirements to control grain structure for the SiC layers of TRISO particles [6]. Based on prior experience, excessively large grains crossing a significant fraction of the SiC layer are undesirable. Furthermore, fundamental materials science principles suggest that excessively small grains may also be undesirable because of enhanced grain boundary diffusion. The precise optimal range of grain size for SiC layers of TRISO particles has not been established, but fuel performance tests have demonstrated ranges where the SiC exhibits the desired behavior. To specifically avoid grain structures suspected of contributing to poor performance of previously tested TRISO fuel by earlier US programs, the AGR program used a qualitative specification for SiC grain structure, based on comparison of SEM images to a visual standard of SiC with unacceptably large grained, columnar microstructure [24].

Advances in automated image analysis for measurement of grain size and the development of benchtop SEM systems capable of rapid sample loading and imaging have made a more quantitative approach to SiC specification and characterization feasible [25]. This method is detailed in Section 2.2. Currently, irradiation or modeling data to support establishing performance-informed limits for SiC grain size are lacking, but the strong irradiation performance of TRISO particles tested under the AGR program may be used as a starting point for a reasonable quantitative specification of SiC microstructure. Data for representative samples from the various AGR irradiation campaigns are provided in Section 2.3. An official data acquisition method has been issued at ORNL, allowing the application of this method at an NQA-1 level of rigor.

2.2 STEPS FOR MEASUREMENT OF SIC MICROSTRUCTURE

2.2.1 Sample Selection

Similar to sample selection for UCO kernel composition measurement, a statistical sampling approach should be employed for measuring SiC microstructure. Whether characterizing a single batch or a composite, a subsample of the appropriate size should be taken from the bulk material by a random representative sampling method such as chute splitting or rotary riffling. The sample's target mass may be set from a known average particle mass and the desired level of statistical sampling. Because the SiC microstructure tends to be fairly uniform within a coating batch and a large number of grains are measured for each particle, a relatively small particle sample is sufficient for SiC microstructure measurement so long as a visual check of a sufficiently large sample of particles is performed by the operator to confirm that the measured particles are representative of the lot.

2.2.2 Mounting and Polishing

Although dedicated materialographic mounts may be produced for measuring SiC microstructure, existing materialographic mounts from other characterization methods can also be used (e.g., optical microscopy mounts for layer thickness measurement or 2-MGEM mounts for pyrocarbon layer anisotropy measurement). Using materialographic mounts initially produced for another characterization method may require some additional polishing steps to optimize SEM image quality. In any case, the mounts should be polished to near midplane so that any trends in grain size from the inner to the outer edges of the SiC layer may be appropriately identified.

2.2.3 Imaging

In this work, the SiC layer of particles was imaged using a Thermo Fisher Scientific Phenom XL desktop SEM instrument. Images were taken at an accelerating voltage of 15 keV with a chamber pressure of 60 Pa. While this instrument is not the most advanced or capable research SEM, it offers an accessible option for an industrial setting. BSE images of the SiC layer were acquired at one point on five particles from each sample measured. The points were selected such that the SiC layer ran from the top to the bottom of the image with the outer and inner edges of the SiC layer captured to the left and right sides of the image. Imaging conditions were selected to maximize contrast between the grains by fully saturating the brightest grains at the maximum intensity while keeping the darkest regions near the minimum intensity. These imaging conditions were first developed for the initial publication on this method for SiC microstructure measurement by BSE imaging [25].

2.2.4 Image Analysis

A range of computational methods may be used to identify grain boundaries in BSE images of SiC for grain size determination based on American Society for Testing and Materials (ASTM) International's method E1382 [26]. For example, Canny edge detection or similar algorithms may be used to identify edges based on local variations in image intensity, or newer machine learning approaches may be used to train neural networks to identify edges in BSE images of SiC based on a set of marked training images. Regardless of how the edges are segmented, the length of grains within a given area is then used with the formulas in E1382 to calculate the average grain size within that area. Note that this method is designed for use with equiaxed grain structures of an appropriate size to be resolved with the imaging settings used. Excessively fine grained SiC or SiC with undesirable columnar microstructure will not be well-characterized by this method.

In this work, the MathWorks MATLAB program described in [25] was applied for image analysis. This program first identifies edges using the Canny edge detection algorithm and then applies several methods to attempt to connect nearby unconnected grain boundaries. Finally, the program calculates the average grain size in circular areas distributed evenly across the image as well as an overall average grain size for the full image. After image processing, a user-review step ensures that the automated algorithm did a reasonable job of segmenting the grain boundaries within the image. In practice, some grain boundaries are always missed and some spurious grain boundaries marked, but in a well-tuned algorithm, these errors will roughly balance out and yield a reasonably accurate measure of the average grain size.

In addition to average grain area, the ratio of mean grain size along the outer and inner edges of the SiC layer is reported for the samples measured. In SiC deposition, grains tend to begin small during initial nucleation and then grow wider as the deposition proceeds. This metric is one way to quantify the variation in average grain area across the coating layer. Finally, an orientation factor is also reported as a potential means to identify columnar grains with a preferred orientation (e.g., across the SiC layer). This orientation factor was calculated by taking the ratio of grain boundary intersections per unit length.

2.3 EXAMPLE SIC MICROSTRUCTURE RESULTS FOR AGR PARTICLES

2.3.1 Legacy Particles

Near the beginning of the AGR program, legacy particles from prior programs were acquired for study. Particles from two of those reference samples were imaged for measurement of SiC microstructure as a part of this work. First, five particles from the General Atomics TRISO particle batch 8876-70 that was used for the HRB-21 irradiation test were imaged [27]. Particles from this batch had previously been characterized at the start of the AGR program to provide reference data for this previously tested UCO fuel [28]. SiC image analysis results are given in Table 4, and a representative image from one of the particles is shown in Figure 17. This batch had relatively coarse-grained SiC with large, columnar grains with internal twins extending across a significant portion of the coating layer. The mean average grain area observed was 0.594 μm^2, and the standard error was 0.015 μm^2, however, these values are not fully representative of the HRB-21 SiC microstructure because it is outside the bounds of the ASTM method. First, the equation used in the ASTM method to determine average grain area from the length of grain boundaries per unit area is based on the assumption of equiaxed grains, not the columnar grain structure visible in Figure 17. Second, the current grain segmentation software does not have the means to separately identify twins from other grain boundaries. This affects both the average grain area as well as the orientation factor, as the twins tend to be aligned perpendicular to the large columnar grains, giving the false appearance of a more even grain orientation. Additional development of the image analysis software is needed to address the presence of twins.

Table 4. SiC grain size data from BSE image analysis for HRB-21 reference particles from batch 8876-70

Sample	Average grain area (μm^2)	Outer/inner grain size ratio	Orientation Factor
Particle 1	0.607	1.88	1.31
Particle 2	0.568	2.43	1.35
Particle 3	0.565	1.56	1.25
Particle 4	0.648	2.18	1.23
Particle 5	0.583	1.60	1.22
Mean	0.594	1.93	1.27

* Note: The columnar and twinned microstructure of HRB-21 SiC is outside the bounds of the ASTM method used to generate these data, so these values are not fully representative of the HRB-21 SiC microstructure.

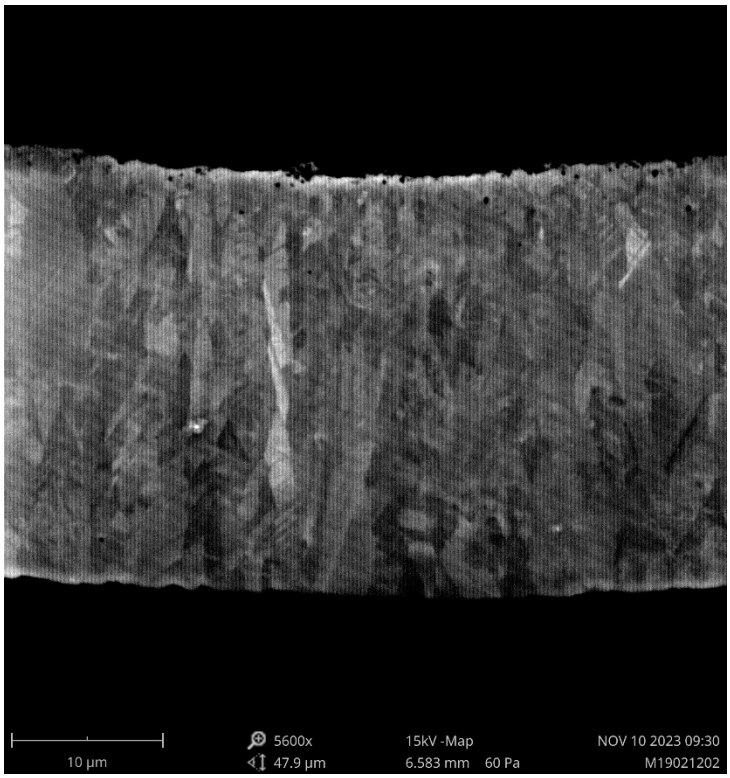

Figure 17. Representative BSE image of the SiC layer of Particle 1 from the batch tested in the HRB-21 irradiation with an unsuitably large and columnar grains.

The second legacy sample measured in this work were five particles from a German proof test composite (EUO 2358–2365) considered representative of the best performing TRISO fuel produced by the German fuel program [29]. Particles from this composite had previously been characterized at the start of the AGR program to provide reference data for this previously tested UO_2 fuel [30]. SiC image analysis results for this material are given in Table 5, and a reference image of a representative SiC layer from these particles is shown in Figure 18. The mean average grain area was 0.415 μm^2, and the standard error was 0.025 μm^2.

Table 5. SiC grain size data from BSE image analysis of German reference fuel

Sample	Average grain area (μm^2)	Outer/inner grain size ratio	Orientation Factor
Particle 1	0.481	1.68	1.23
Particle 2	0.424	1.29	1.41
Particle 3	0.437	1.38	1.26
Particle 4	0.327	1.56	1.28
Particle 5	0.407	1.56	1.21
Mean	0.415	1.49	1.28

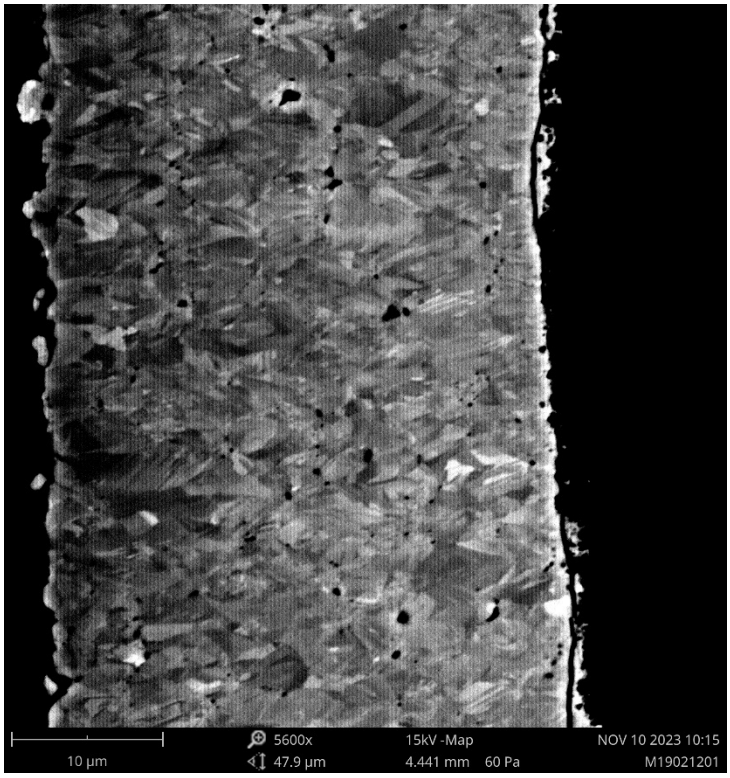

Figure 18. Representative BSE image of the SiC layer of German reference fuel Particle 1 with moderately sized, equiaxed grains.

2.3.2 AGR-1 SiC Analysis

As part of the initial effort to develop an automated image analysis approach for quantitative measurement of SiC microstructure in TRISO particles, a broad study on the different coating batches from the AGR-1 campaign was previously conducted [25]. Batches coated using the Variant 3 parameters from the AGR-1 campaign are of particular interest, as these coating parameters, which included argon dilution during SiC deposition, were designed to produce a finer grained SiC layer compared with the baseline coating conditions, and argon-dilution was used for subsequent AGR-2 and AGR-5/6/7 campaigns. Data for particles from AGR-1 Baseline batch LEU01-35T and AGR-1 Variant 3 batch LEU01-24T are given in

Table 6 and Table 7 and representative BSE images are shown in Figure 19 and Figure 20. The impact of the Variant 3 coating parameters is evident, as the mean average grain area decreased from 0.565 μm^2 with a standard error of 0.011 μm^2 for the Baseline batch down to 0.336 μm^2 with a standard error of 0.008 μm^2 for the Variant 3 batch.

Table 6. SiC Grain size data from BSE image analysis of AGR-1 Baseline batch LEU01-35T

Sample	Average grain area (μm^2)	Outer/inner grain size ratio	Orientation Factor
Particle 1	0.494	1.26	1.47
Particle 2	0.570	1.86	1.45
Particle 3	0.555	1.66	1.48
Particle 4	0.549	1.54	1.48
Particle 5	0.552	1.48	1.50
Particle 6	0.658	2.14	1.60
Particle 7	0.567	1.43	1.53
Particle 8	0.590	1.78	1.48
Particle 9	0.541	1.49	1.52
Particle 10	0.524	1.67	1.50
Particle 11	0.525	2.05	1.56
Particle 12	0.627	1.80	1.56
Particle 13	0.600	1.65	1.45
Particle 14	0.582	1.69	1.44
Particle 15	0.544	1.74	1.45
Mean	0.565	1.683	1.498

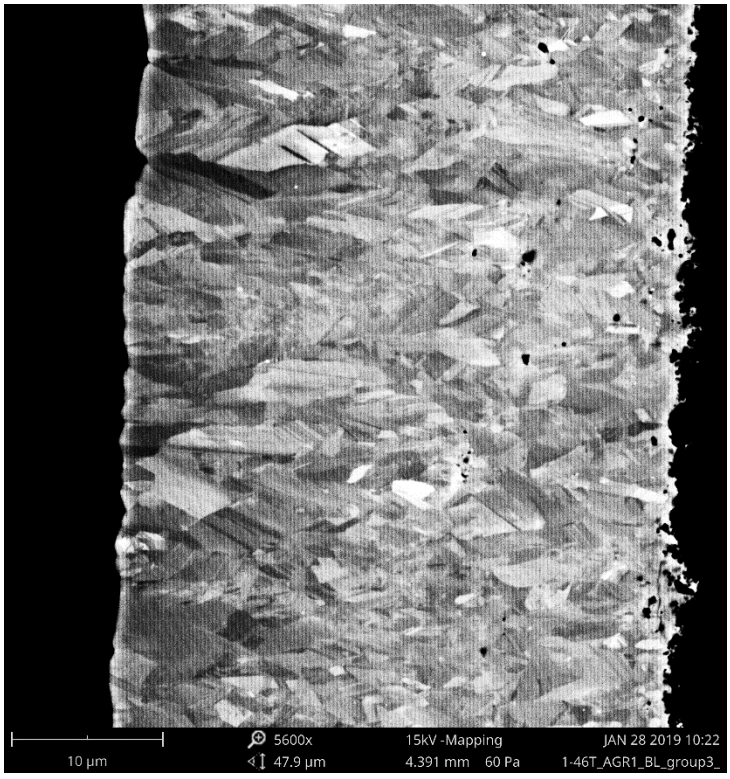

Figure 19. Representative BSE image of the SiC layer of Particle 2 from AGR-1 Baseline LEU01-35T with moderately sized, equiaxed grains.

Table 7. SiC grain size data from BSE image analysis of AGR-1 Variant 3 batch LEU01-24T

Sample	Average grain area (μm^2)	Outer/inner grain size ratio	Orientation Factor
Particle 1	0.375	1.31	1.28
Particle 2	0.320	1.33	1.23
Particle 3	0.396	1.48	1.17
Particle 4	0.327	1.70	1.25
Particle 5	0.303	1.43	1.26
Particle 6	0.332	1.47	1.29
Particle 7	0.340	1.44	1.15
Particle 8	0.306	1.42	1.24
Particle 9	0.331	1.61	1.29
Particle 10	0.389	1.34	1.30
Particle 11	0.319	1.28	1.28
Particle 12	0.333	1.32	1.19
Particle 13	0.302	1.51	1.21
Particle 14	0.336	1.40	1.26
Mean	0.336	1.43	1.24

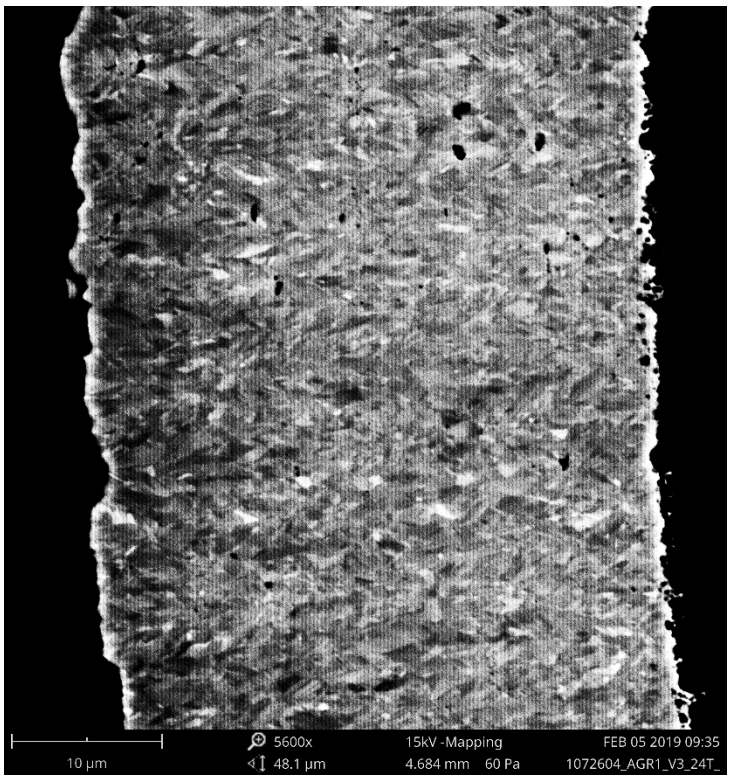

Figure 20. Representative BSE image of the SiC layer of Particle 6 from AGR-1 Variant 3 Batch LEU01-24T with a fine-grained equiaxed structure.

2.3.3 AGR-2 SiC Analysis

Regions of the SiC layer of five different AGR-2 particles from LEU09-B01 were imaged and analyzed to determine average SiC grain size. The overall average grain area and the ratio of the grain area at the outer edge of the layer to the inner edge of the layer are given in Table 8. An example BSE image of the SiC layer of one particle is shown in Figure 21. The mean grain area measured by BSE image analysis for AGR-2 particles was 0.431 μm^2, and the standard error was 0.003 μm^2. This result is comparable to the German reference particles.

Table 8. SiC grain size data from BSE image analysis of AGR-2 sample

Sample	Average grain area (μm^2)	Outer/inner grain size ratio	Orientation Factor
Particle 1	0.434	2.72	1.32
Particle 2	0.437	2.03	1.30
Particle 3	0.433	2.12	1.29
Particle 4	0.431	1.73	1.32
Particle 5	0.419	1.49	1.34
Mean	0.431	2.02	1.32

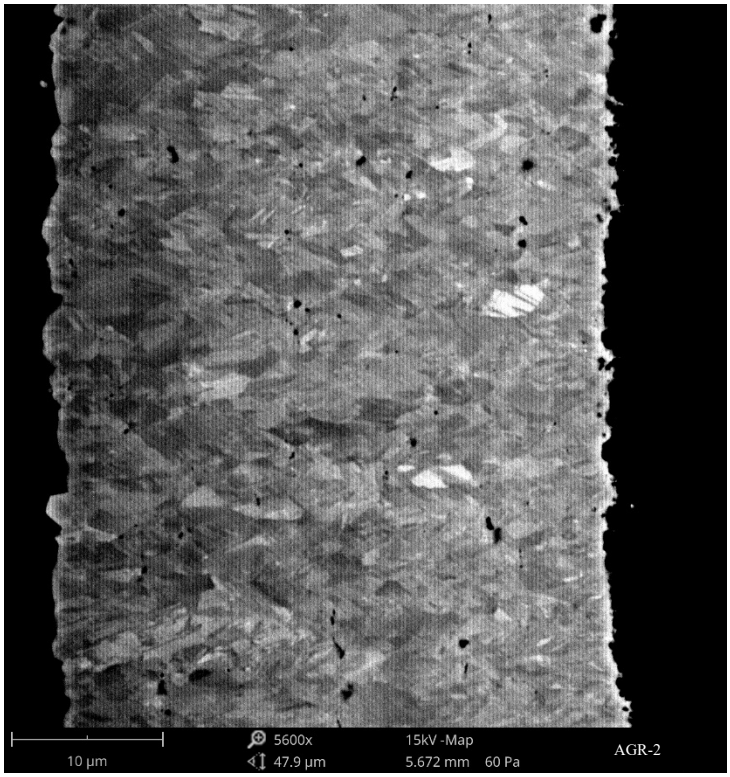

Figure 21. Representative BSE image of the SiC layer of AGR-2 Particle 4 with moderately sized, equiaxed grains.

2.3.4 AGR-3/4 SiC Analysis

Regions of the SiC layer of five different AGR-3/4 particles from LEU03-10T were imaged and analyzed to determine average SiC grain size. The overall average grain area and the ratio of the grain area at the

outer edge of the layer to the inner edge of the layer are given in Table 9. Example images of the relatively fine and coarse structures observed in the AGR-3/4 sample are shown in Figure 22 and Figure 23. The mean grain area measured by BSE image analysis for AGR-1 particles was 0.581 μm^2, and the standard error was 0.077μm^2.

Table 9. SiC grain size data from BSE image analysis for AGR-3/4 sample

Sample	Average grain area (μm^2)	Outer/inner grain size ratio	Orientation Factor
Particle 1	0.672	2.86	1.47
Particle 2	0.361	5.02	1.35
Particle 3	0.755	2.88	1.35
Particle 4	0.434	2.56	1.19
Particle 5	0.684	5.30	1.38
Mean	0.581	3.73	1.35

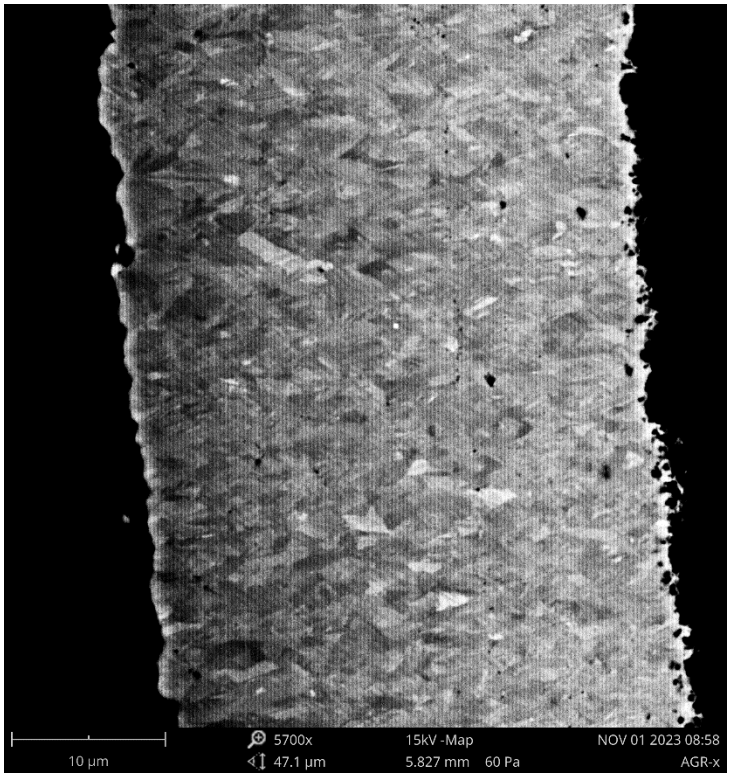

Figure 22. Representative BSE image of the SiC layer of Particle 2 from AGR-3/4 Composite LEU03-10T with a fine, equiaxed grain structure.

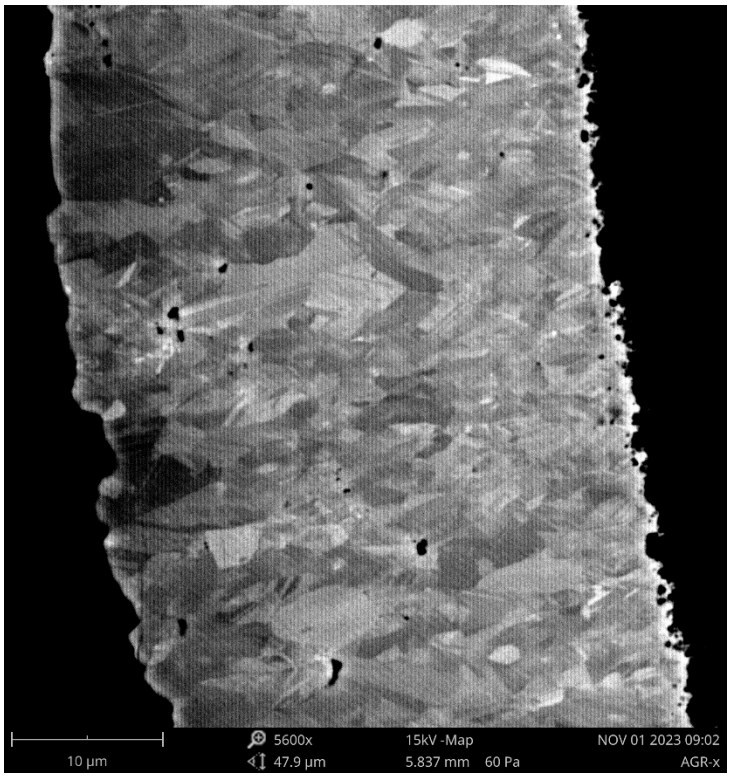

Figure 23. Representative BSE image of the SiC layer of Particle 3 from AGR-3/4 Composite LEU03-10T with a coarse, equiaxed grain structure.

The initial results for average SiC grain size for AGR-3/4 particles in Table 9 indicate a bimodal distribution with two particles having an average grain area of about 0.4 μm^2 and the other three having an average grain area of about 0.7 μm^2. To confirm whether the apparent variation in average SiC grain size was interparticle or intraparticle, two additional AGR-3/4 particles were imaged at four separate locations around the SiC layer. These results are given in Table 10. Both particles showed reasonable consistency in the measured SiC grain area at the four points selected; however, the particles clearly had different SiC microstructure. Archived samples of the individual batches are no longer available for analysis to better determine the variation between batches; however, this data would not likely be of substantial use anyway, as there is relatively little driver fuel performance data for AGR-3/4 due to the inclusion of designed-to-fail particles in this experiment.

AGR-3/4 SiC was deposited without argon dilution using conditions similar to AGR-1 Baseline, which also exhibited batch-to-batch variation in SiC microstructure. Batch LEU01-45T, included in the AGR-1 Baseline composite, had a noticeably smaller image analysis-determined average grain size (0.472 μm^2) compared with the other three AGR-1 Baseline batches (0.581–0.653 μm^2) that was clearly evident when performing either EBSD or BSE quantitative analysis [31, 25]. During the QC acceptance testing of this material, some grain size variation was observed, but it was not noted as a concern as it did not impact the conclusion that all the material was clearly deemed acceptable when qualitatively compared to the visual standard [10]. However, with the higher fidelity of the quantitative analysis methods, such batch-to-batch variation is easily resolved and can impact the normality of the data set when analyzing a multi-batch composite. Therefore, quantified SiC grain size inspection may be more appropriately applied at the batch level when such batch-to-batch variation exists.

Table 10. SiC grain size data from BSE image analysis repeated at multiple locations on two AGR-3/4 particles

Sample	Average grain area (μm²)	Outer/inner grain size ratio	Orientation Factor
Particle 6	0.652	3.48	1.47
Particle 6	0.623	3.09	1.35
Particle 6	0.549	2.47	1.26
Particle 6	0.572	2.29	1.38
Particle 6 mean	0.599	2.83	1.36
Particle 7	0.346	1.69	1.38
Particle 7	0.395	1.56	1.28
Particle 7	0.380	1.76	1.31
Particle 7	0.409	1.41	1.21
Particle 7 mean	0.383	1.60	1.30

2.3.5 AGR-5/6/7 SiC Analysis

Regions of the SiC layer of five different AGR-5/6/7 particles from compact AGR 5/6/7-1230 were imaged and analyzed to determine average SiC grain size. The overall average grain area and the ratio of the grain area at the outer edge of the layer to the inner edge of the layer are given in Table 11. An example raw image, segmented image, and surface map of the variation of average grain size across one of the particles from AGR-5/6/7 are shown in Table 11. The mean grain area measured by BSE image analysis for AGR-5/6/7 particles was 0.313 μm², and the standard error was 0.013 μm². This mean grain area is notably smaller than that of LEU01-35T (AGR-1 Baseline) and AGR-2 particles, and the difference in microstructure can be noted visually as well by comparing Figure 19 and Figure 21 with Figure 24. Although the mean average grain area of AGR-5/6/7 SiC was measured to be only slightly lower than AGR-1 Variant 3 SiC, visual comparison of Figure 20 and Figure 24 suggests the actual microstructure of the AGR-5/6/7 SiC is more fine. This discrepancy between quantitative and qualitative comparison may be due to the AGR-5/6/7 microstructure reaching the lower-limit of grains which can be resolved with the imaging settings used. This could be remedied by imaging with a higher quality SEM at greater magnification; however, that may be unnecessary so long as the system used can accurately resolve grain boundaries down to whatever lower bound on SiC grain size may be specified.

Table 11. SiC grain size data from BSE image analysis for AGR-5/6/7 sample

Sample	Average grain area (μm²)	Outer/inner grain size ratio	Orientation Factor
Particle 1	0.353	2.02	1.05
Particle 2	0.292	1.94	1.10
Particle 3	0.278	2.34	1.14
Particle 4	0.313	1.88	1.18
Particle 5	0.331	2.15	1.08
Mean	0.313	1.95	1.12

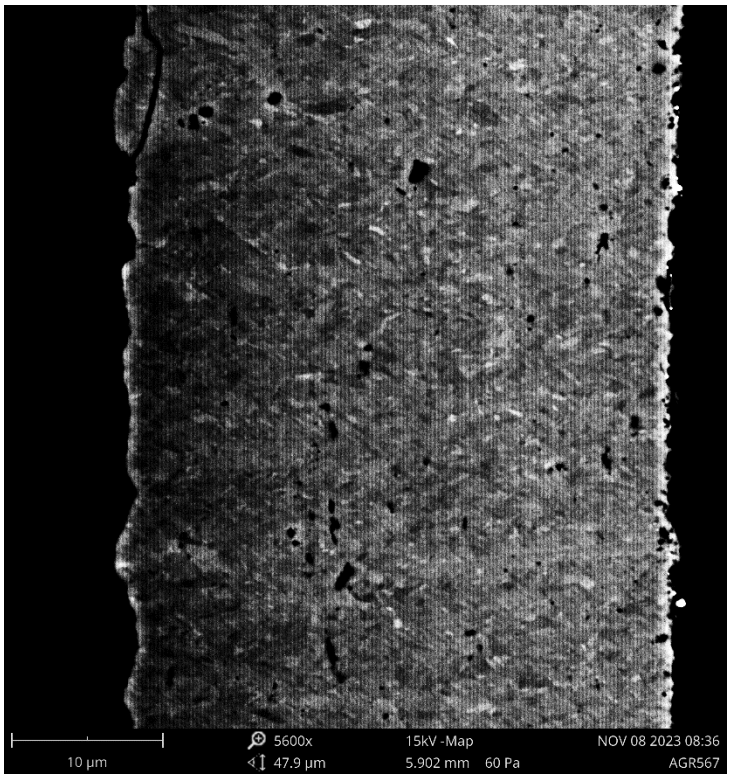

Figure 24. Representative BSE image of the SiC layer of Particle 4 from AGR-5/6/7 with a fine-grained, equiaxed structure.

2.4 SIC MICROSTRUCTURE MEASUREMENT SUMMARY

The method initially described in [25] for measurement of SiC layer microstructure using automated analysis of BSE images has been formalized as an ORNL procedure, allowing for general application to TRISO particles. This method generates quantitative data on the average SiC grain size. This method may replace the previously used qualitative visual standard approach for SiC microstructure specification. Application of this method to legacy samples as well as representative samples from the four AGR irradiation campaigns demonstrates its applicability and provides some interesting insights into the variations in microstructure between these materials. Notably, particles from AGR-1 Baseline Batch LEU01-35T and AGR-2 had SiC microstructures similar to the legacy German TRISO particles: average grain area was about 0.47 μm^2. Particles from AGR-3/4 showed a bimodal distribution of SiC microstructure, which was also observed previously for one of the AGR-1 Baseline batches. Finally, particles from AGR-5/6/7 had a finer SiC microstructure than particles from the prior irradiation campaigns: average grain area was about 0.313 μm^2. A summary of the results for SiC microstructure for all samples analyzed is given in

Table 12. Data for HRB-21 is not included in Table 13 due to the previously noted incompatibility of the columnar, twinned microstructure with the analysis method.

Table 12. Summary of results for quantification of SiC microstructure for legacy and AGR particles

Material	Average grain area (μm²)		
	Mean	Standard Deviation	Standard Error
German Reference	0.415	0.056	0.025
AGR-1 Baseline (35T)	0.565	0.042	0.011
AGR-1 Variant 3 (24T)	0.336	0.030	0.008
AGR-2	0.431	0.007	0.003
AGR-3/4	0.581	0.173	0.077
AGR-5/6/7	0.313	0.030	0.013

2.5 SIC MICROSTRUCTURE IMAGE ANALYSIS CONCLUSIONS AND RECOMMENDATIONS

The automated BSE image analysis method based on ASTM E1382 and presented herein provides an industrially applicable approach to quantify the size of the SiC microstructure in TRISO particles. However, this approach has several important limitations when considering its implementation as part of a specification on SiC microstructure. First, as seen for the HRB-21 data, the current image analysis method does not adequately identify large, columnar grains due to false-positive grain boundaries introduced by twinning. Second, as seen for the AGR-3/4 data, application of SiC grain size measurement at the composite level is likely not the best approach due to potential variation in SiC properties between coating batches. Third, as seen for the AGR-5/6/7 data, a very fine microstructure may exceed the resolution limit of the images for grain boundary detection, resulting in an inaccurate grain size measurement. Each of these limitations may be addressed in a carefully developed specification on SiC microstructure and by using an informed application of the method to look for these limiting cases.

Samples with excessively large columnar grains and twinning, which are clearly evident in the BSE images, may be rejected by a qualitative step based on operator judgement or identified by improved image segmentation methods. The currently applied image segmentation is based on edge detection of contrast variations in the BSE images due to grain orientation and readily identifies twins as grain boundaries; however, a more advanced machine-learning based approach to grain segmentation can be trained on data sets in which twins have been correctly labeled. This improvement in grain segmentation would likely enable the establishment of quantitative limits on the size and aspect ratio of columnar grains relative to the width of the SiC layer, while also supporting the current ASTM approach for determination of average grain area based on the density of grain boundaries for appropriately equiaxed samples.

The need to perform an assessment of SiC microstructure at the batch level is not onerous, as coating layers thicknesses are typically specified and measured at the batch level already. The same materialographic mounts may be used for both processes, potentially with an additional polishing step between optical and SEM imaging to optimize the surface of the SiC. The typical layer thickness mount with hundreds of particles would be more than sufficient for a qualitative survey to ensure that the SiC layers of the particles selected for SEM imaging and analysis are representative of the whole batch. The number of particles which should be quantitatively analyzed will need to be established based on the typical level of variation within a batch and on tests for normality associated with the statistical sampling of variable properties. If the SiC grain size is considered as a variable property, then a sufficient number of particle layers should be analyzed to satisfy requirement for normality in the measured distribution.

Finally, the limitation of a lower resolution limit for grain boundary detection is not a challenge so long as that lower resolution limit is comfortably below the specified lower limit (if any) on the SiC grain size. If no lower limit on SiC grain size is specified, then the associated characterization method will only need to show that the grain size is below the upper limit, and a lower resolution limit will not be an issue. However, if a lower resolution limit is specified due to enhanced grain boundary diffusion for very fine-grained SiC, then the imaging settings and analysis method will need to be qualified to confirm the capability to resolve grains down to that limit.

3. REFERENCES

[1] D. Petti, J. Maki, J. Hunn, P. Pappano, C. Barnes, J. Saurwein, S. Nagley, J. Kendall and R. Hobbins, "The DOE Advanced Gas Reactor Fuel Development and Qualification Program," *JOM,* vol. 62, no. 9, pp. 428-441, 2010.

[2] D. Petti and J. Maki, "The Challenges Associated with High Burnup and High Temperature for UO2 TRISO coated Particle Fuel," INL/CON-05-00038, Idaho National Laboratory, Idaho Falls, ID, 2005.

[3] R. N. Morris, J. D. Hunn, C. A. Baldwin, F. C. Montgomery, T. J. Gerczak and P. A. Demkowicz, "Initial results from safety testing of US AGR-2 irradiation test fuel," *Nuclear Engineering and Design,* vol. 329, pp. 124-133, 2018.

[4] M. Wagner-Loffler, "Amoeba Behavior of UO2 Coated Particle Fuel," *Nuclear Technology,* vol. 35, no. 2, 1977.

[5] J. W. McMurray, T. B. Lindemer, N. R. Brown, T. J. Reif, R. N. Morris and J. D. Hunn, "Determining the minimum required uranium carbide content for HTGR UCO fuel kernels," *Annals of Nuclear Energy,* vol. 104, pp. 237-242, 2017.

[6] P. Demkowicz, D. Marshall and J. Hunn, "Advanced Gas Reactor Fuel Specification Technical Bases," INL/RPT-23-71992, Idaho National Laboratory, Idaho Falls, 2023.

[7] G. Helmreich, J. Hunn, J. McMurray and D. Brown, "Enhanced method for analysis of individual UCO kernel phase fractions," *Nuclear Engineering and Design,* vol. 363, 2020.

[8] "LEU Kernel Lot 69302 Data Package," BWX Technologies, Lynchburg, 2005.

[9] "Composition Distribution of Fuel Kernels in LEU Composite 69302," EDF-5723, BWX Technologies, Lynchburg, 2005.

[10] J. Hunn and R. Lowden, "Data Compilation for AGR-1 Baseline Coated Particle Composite LEU01-46T," ORNL/TM-2006/019-R1, Oak Ridge National Laboratory, Oak Ridge, 2006.

[11] A. Kercher and J. Hunn, "Results from ORNL characterization of nominal 350 um LEUCO kernels from BWXT G73D-20-69302 composite," ORNL/TM-2005/517, Oak Ridge National Laboratory, Oak Ridge, 2005.

[12] J. Phillips, C. Barnes and J. Hunn, "Fabrication and Comparison of Fuels for Advanced Gas Reactor Irradiation Tests," in *Proceedings of HTR 2010 5th International Topical Meeting on High Temperature Reactor Technology*, Prague, October 18-20, 2010.

[13] "LEU Kernel Lot 69307 Data Package," BWX Technologies, Lynchburg, 2008.

[14] "LEU Kernel Lot 69303 Data Package," BWX Technologies, Lynchburg, 2006.

[15] M. Ebner and C. Barnes, "UCO Kernel Fabrication Development for the Advanced Gas Reactor Program," INL/EXT-07-12247, Idaho National Laboratory, Idaho Falls, 2007.

[16] A. Kercher and J. Hunn, "Results from ORNL characterization of nominal 350 um LEUCO kernels (LEU03) from the BWXT G73V-20-69303 composite," ORNL/TM_2006/552, Oak Ridge National Laboratory, Oak Ridge, 2006.

[17] J. Hunn and R. Lowden, "Data compilation for AGR-3/4 driver coated particle composite LEU03-09T," ORNL/TM-2007/019, Oak Ridge National Laboratory, Oak Ridge, 2007.

[18] D. Marshall, "AGR-5/6/7 Fuel Fabrication Report," INL/EXT-19-53720, Idaho National Laboratory, Idaho Falls, 2019.

[19] "Lot J52R-16-69317 Certification Package," BWX Technologies, Lynchburg, 2016.

[20] J. Hunn, A. Kercher, P. Menchhofer and J. Price, "Results from ORNL Characterization of Nominal 350 um NUCO Kernels from the BWXT 59344 Batch," ORNL/TM-2005/541, Oak Ridge National Laboratory, Oak Ridge, 2005.

[21] B. Toby and R. von Dreele, "GSAS-II: the genesis of a modern open-source all purpose crystallography software package," *Journal of Applied Crystallography,* vol. 46, no. 2, pp. 544-549, 2013.

[22] A. Larson and R. Von Dreele, "General Structure Analysis System (GSAS)," LAUR 86-748, Los Alamos National Laboratory, Los Alamos, 2004.

[23] R. Jones, "Uranium Carbide as a Nuclear Fuel," International Atomic Energy Agency, Vienna, Austria, 1972.

[24] D. Marshall, "AGR-5/6/7 Fuel Specification," SPC-1352, Rev. 8, INL/MIS-11-21423, Idaho National Laboratory, Idaho Falls, 2017.

[25] G. Helmreich, D. Brown, T. Gerczak and J. Hunn, "Quantification of silicon carbide grain structure in TRISO fuel by BSE image analysis," *Journal of Nuclear Materials,* vol. 533, 2020.

[26] "ASTM E1382 Standard test methods for determining average grain size using semiautomatic and automatic image analysis," ASTM International, West Conshohocken, PA, 2015.

[27] C. Young, "Capsule HRB-21 Preirradiation Report," DOE-HTGR-88357, General Atomics, 1991.

[28] J. Hunn, "Results from ORNL Characterization HRB-21 Reference Fuel," ORNL/TM-2005/544, Oak Ridge National Laboratory, Oak Ridge, 2005.

[29] J. Saurwein, "Acceptance Test Report for German Fuel Particles," GA-910852, General Atomics, 1995.

[30] J. Hunn, "Results from ORNL Characterization of German Reference Fuel from EUO 2358-2365 Composite," ORNL/TM-2005/546, Oak Ridge National Laboratory, Oak Ridge, 2005.

[31] T. Gerczak, J. Hunn and R. A. T. Lowden, "SiC Layer Microstructure in AGR-1 and AGR-2 TRISO Fuel Particles and the Influence of its Variation on the Effective Diffusion of Key Fission Products," *Journal of Nuclear Materials,* vol. 480, pp. 1-14, 2016.